J. Biochem. 2009;146(1)33–41
doi:10.1093/jb/mvp041

High-Sensitivity Analysis of Naturally Occurring Sugar Chains, Using a Novel Fluorescent Linker Molecule

Masaki Sato[1], Yuji Ito[2], Naomichi Arima[3], Masanori Baba[3], Michael Sobel[4], Masahiro Wakao[1] and Yasuo Suda[1,5,*]

[1]Department of Nanostructure and Advanced Materials; [2]Department of Bioengineering, Graduate School of Science and Engineering, Kagoshima University, 1-21-40, Kohrimoto, Kagoshima 890-0065; [3]Center for Chronic Viral Diseases, Graduate School of Medical and Dental Sciences, Kagoshima University, Japan; [4]Department of Surgery, VA Puget Sound HCS and The University of Washington School of Medicine, Seattle, WA, USA; and [5]SUDx-Biotec Corp., 1-42-1, Shiroyama, Kagoshima, 890-0013, Japan

Received February 16, 2009; accepted February 26, 2009; published online March 6, 2009

To analyse the binding of sugar chains to proteins, viruses and cells, the surface plasmon resonance (SPR) technique is very convenient and effective because it is a real-time, non-destructive detection system. Key to this method is linker compounds for immobilization of the sugar chains to the gold-coated chip for SPR. Also, well-designed fluorescent labelling reagents are essential when analysing the structure of trace amounts of sugar chains derived from natural sources, such as glycoproteins on the surface of specific cells. In this report, we developed a novel linker molecule, named 'f-mono', which has both of these properties: simple immobilization chemistry and a fluorescent label. Since the molecule contains a 2,5-diaminopyridyl group and a thioctic acid group, conjugation with sugar chains can be achieved using the well-established reductive amination reaction. This conjugate of sugar chain and fluorescent linker (fluorescent ligand-conjugate, FLC) has fluorescent properties (ex. 335 nm, em. 380 nm), and as little as 1 μg of FLC can be easily purified using HPLC with a fluorescent detector. MS and MS/MS analysis of the FLC is also possible. As a +2 Da larger MS peak ($[M+H+2]^+$ ion) was always associated with the theoretical MS peak ($[M+H]^+$) (due to the reduction of the thioctic acid moiety), the MS peaks of the FLC were easily found, even using unfractionated crude samples. Immobilization of the FLC onto gold-coated chips, and their subsequent SPR analyses were successively accomplished, as had been performed previously using non-fluorescent ligand conjugates.

Key words: immobilization, sugar chain, high sensitivity, analysis, fluorescence, linker molecule, mass spectrometry.

Abbreviations: DMAc, N, N-dimethyl acetoamide; aoWS, N^{α}-((aminooxy)acetyl)tryptophanylarginine methyl ester.

The carbohydrates that make up proteoglycans, glycoproteins or glycolipids are responsible for many biological functions and play crucial roles in cellular binding and signalling (*1*). However, because of their structural complexity, the methods for studying sugar chains are more challenging than that for DNA, RNA or proteins. The numerous isomeric and anomeric configurations of sugar chains, as well as the difficulties in isolating sufficient quantities of naturally occurring sugars, make binding analysis and structure–function studies challenging.

For the structural analysis of naturally occurring sugar chains, fluorescent labelling of the sugars has been one popular technique (*2*). Recently, mass spectrometry (MS) has been used for structural analysis of sugar structures, thanks to the development of structurally well-defined standards (*3*, *4*). Surface plasmon resonance (SPR) methodology is also a very effective method to quantify binding interactions between sugar-chains and lectins or viruses in real time, because it is a non-destructive technology that does not require large quantities of the often scarce materials to be studied (*5–9*). We have previously reported the development of the 'sugar chip', in which defined sugar chains are immobilized on an SPR sensor chip using our specialized linker molecules (*10*, *11*). But the purification of these linker-carbohydrate conjugates for SPR has been difficult when the quantities of the target sugar chains were limited (*i.e.* <1 mg). To overcome this and the other challenges in the analysis of scarce sugar chains, we have developed a novel carbohydrate linker molecule that is also fluorescent (named 'f-mono'). Here we report the successful synthesis of this novel fluorescent linker molecule, and the preparation and purification of conjugates (fluorescent ligand-conjugate or FLC) using as little as 1 μg of sugar chain. These FLCs were then effectively employed in SPR analysis of carbohydrate–protein binding, as well as MS and MS/MS structural analyses.

MATERIALS AND METHODS

General Procedure—All reactions in organic media were carried out with freshly distilled solvents or with

*To whom correspondence should be addressed. Tel: +81-99-285-8369, Fax: +81-99-285-8369, E-mail: ysuda@eng.kagoshima-u.ac.jp

commercially available extra grade solvents purchased from Kanto Chem. Co. (Tokyo, Japan), Nacalai Tesque (Kyoto, Japan) or Wako Chem. Co. (Osaka, Japan). Silica gel column chromatography was performed using PSQ 60B (Fuji Silysia Chem. Ltd., Aichi, Japan). Electrospray ionization time-of-flight mass (ESI-TOF/MS) spectra were obtained by Mariner™ (Applied Biosystems, Framingham, MA, USA). ^{1}H-NMR measurements were performed with JEOL (Tokyo, Japan) ECA-600.

Synthesis of f-mono linker—2,6-Diaminopyridine (1.06 g, 9.70 mmol, Sigma, USA) and thioctic acid (1.00 g, 4.80 mmol, Sigma, USA) were dissolved in anhydrous *N, N*-dimethylformamide (10 ml). Then, 1-hydroxy-7-azabenzotriazole (HOAt, 0.66 g, 4.80 mmol), 1-ethyl-3-(3-dimethylaminopropyl)carbodiimide monohydrochloride (EDC-HCl, 0.93 g, 4.80 mmol), and diisopropylethylamine (DIEA, 0.84 ml, 4.80 mmol) were added to the solution. After stirring for 6 h under argon gas, the reaction product was extracted into the organic phase using dichloromethane (CH_2Cl_2, 20 ml), and was washed with water (10 ml) three times and then with saturated sodium bicarbonate aqueous solution. The product was then purified by silica gel column chromatography (80 g, eluted with toluene/ethyl acetate = 3/1, v/v) to obtain a yellow solid. Yield: 1.37 g (95%). MS calcd. for $C_{13}H_{19}N_3OS_2$: 297.10, Found: *m/z* 298.12 $[M+H]^+$; ^{1}H NMR (600 MHz, CDCl3), δ7.58 (1H, s), 7.53 (1H, d, J = 7.5 Hz), 7.46 (1H, t, J = 7.6, J = 8.2 Hz), 6.26 (1H, d, J = 8.2 Hz), 4.24 (1H, m), 3.59–3.56 (1H, m), 3.19–3.10 (2H, m), 2.48–2.44 (1H, m), 2.37–2.34 (2H, m), 1.93–1.90 (1H, m), 1.77–1.68 (4H, m), 1.53–1.48 (2H, m).

Preparation of a Conjugate with Lactose—Lactose monohydrate (20 mg, 56 μmol) and f-mono (18 mg, 61 μmol) were dissolved in a 2.2 ml solution of H_2O/AcOH/DMAc = 5/1/5 (v/v/v). After stirring for 5 h, sodium cyanoborohydrate (17 mg, 280 μmol) was added to the solution. The reaction mixture was left standing at 37°C for 1.5 days and lyophilized. The residue was dissolved in water and purified with an ODS column (20 g, 1.8 cmΦ × 46 cm, eluted with water/methanol = 1/1, v/v). The appropriate fraction was lyophilized with water to obtain the desired final product: fluorescent ligand-conjugate (FLC, abbreviated as Galβ1-4Glc-f-mono) as a white powder. Yield: 19 mg (50%). MS calcd. for $C_{25}H_{41}N_3O_{11}S_2$: 623.17, Found: m/z 624.17 $[M+H]^+$; ^{1}H NMR (600 MHz, MeOD), δ 7.31 (1H, d, J = 8.1 Hz), 6.99 (1H, d, J = 2.0 Hz), 6.20 (1H, d, J = 8.0 Hz), 4.28 (1H, d, H-1′), 3.89 (1H, dd, H-4), 3.75 (2H, m, H-2, H-5), 3.63 (3H, m, H-3, H-6a, H-6b), 3.52 (1H, m), 3.45 (1H, m, H-4′), 3.30 (2H, m, H-3′, H-5′), 3.25–3.14 (2H, m, H-1a,H-2′), 3.05–2.94 (3H, m, H-1b), 2.36 (1H, m), 2.26 (2H, t, J = 7.3 Hz), 1.84–1.76 (1H, m), 1.54–1.35 (6H, m).

Preparation of a Conjugate with Maltose—Maltose (20 mg, 56 μmol) and f-mono (18 mg, 61 μmol) were dissolved in a 2.2 ml solution of H_2O/AcOH/DMAc = 5/1/5 (v/v/v). After stirring for 5 h, sodium cyanoborohydrate (17 mg, 280 μmol) was added to the solution. The reaction mixture was left standing at 37°C for 1.5 days, and lyophilized. The residue was dissolved in water and purified with ODS column (20 g, 1.8 cmΦ × 46 cm, eluted with water/methanol = 1/1, v/v). The appropriate fraction was lyophilized with water to obtain Glcα1-4Glc-f-mono as a white powder. Yield: 17 mg (46%). MS calcd. for $C_{25}H_{41}N_3O_{11}S_2$: 623.17, Found: m/z 624.17 $[M+H]+$; ^{1}H NMR (600 MHz, MeOD), δ 7.32 (1H,d), 6.99 (1H, d), 6.20 (1H, d), 4.95 (1H, s, H-1′), 3.89–3.78 (3H, m, H-2, H-4, H-5), 3.63 (3H, m, H-3, H-6a, H-6b), 3.42 (1H, m), 3.38 (1H, d, H-4′), 3.13 (2H, m, H-3′, H-5′), 2.85–2.3 (5H, m, H-1a,H-2′), 3.05–2.94 (3H, m, H-1b), 2.36 (1H, m), 1.74–1.26 (7H, m).

SPR Analysis—SPR experiments were perfomed with a 12-channel SPR machine (Moritex Co., Yokohama, Japan) using the manufacturer's recommended guidelines with slight modification. Sensor chips used for SPR experiments were prepared as follows. The gold-coated chip was purchased from SUDx-Biotec (Kagoshima, Japan), and washed in ozone cleaner. The chip was soaked in a 10-, 1-, or 0.1-μM solution of Galβ1-4Glc-f-mono or Glcα1-4Glc-f-mono, dissolved in methanol/water = 1/1 (v/v) at room temperature for 2 h or overnight, followed by subsequent washing with a methanol/water (1/1, v/v) containing 0.05% Tween-20, phosphate-buffered saline (PBS) at pH 7.4 containing 0.05% Tween-20, and PBS (pH 7.4). All washings were done with ultra-sonication for 20 min.

Binding studies were performed between test proteins in the aqueous phase and the stated sugars immobilized via fluorescent linkers (f-mono) attached to the sugar chips. The test proteins concanavalin A (Con A, EY Laboratories, San Mateo, CA, USA), RCA120 (Ricinus Communis Agglutinin I, Vector Laboratories, Servion, Switzerland), and bovine serum albumin (BSA, Nakalai Tesque) were perfused in the aqueous phase (PBS with 0.05% Tween-20 at pH 7.4) at a flow rate of 15 μl/min at 25°C.

Fluorescent Spectra—Fluorescent spectra were measured with a Spectro Fluorometer FP-6310 (JASCO, Tokyo, Japan). The concentration of f-mono was 100 μg/ml in $CHCl_3$. For comparison, our previous mono-valent non-fluorescent linker molecule [abbreviated as 'mono' in this paper (*11*)] was dissolved in $CHCl_3$ at 100 μg/ml, and used as a control.

Mass Spectrometry—MS and MS/MS spectra of FLCs were obtained with an AXIMA-QIT (Shimadzu, Kyoto, Japan), which is a quadrupole ion trap and matrix-assisted laser desorption/ionization time-of-flight mass spectrometer (QIT-MALDI-TOF/MS). Acquisition and data processing were controlled by the manufacturer's software (Kratos Analytical, Manchester, UK). For matrix, a purified 2,5-dihydroxybenzoic acid (DHBA) was dissolved in a mixed solvent with double distilled water containing 0.1% TFA/acetonitrile = 3/1 (v/v) at 10 mg/ml. To 1 μl of sample dissolved in the above mixed solvent spotted on a stainless-steel target, an equal volume of matrix solution was placed and allowed to dry.

Preparation of f-mono-Labelled Glycans from Human IgG—One hundred micrograms of human IgG (Institute of Immunology Co., LTD., Tokyo, Japan) was dissolved in 5 μl of H_2O and 5 μl of 1 M aqueous NH_4HCO_3, and 5 μl of 120 mM aqueous dithiothreitol were added. The reaction solution was heated at 60°C for 30 min. Then, 10 μl of 123 mM aqueous iodoacetamide was added. After incubation in the dark at room temperature for an hour, 10 μl of

trypsin (Sigma-Aldrich, 40 U/μl, dissolved in 1 mM HCl) was added. After an hour, trypsin was inactivated by heating at 90°C for 5 min. Then, 10 U of PNGase F (Roche, Switzerland) was added to the solution (*12*). After incubating at 37°C for 12 h, the solution was lyophilized.

The lyophilized residue was dissolved in 20 μl of H_2O, and concentrated by Blot Glyco (Kit No. MALDI type BS-45601S, Sumitomo Bakelite Co., Ltd. Tokyo, Japan) (*13*, *14*). At the final stage, using the manufacturer's guideline, N-glycans from IgG were released in H_2O, lyophilized and transformed to fluorescent ligand conjugates as follows. The mixture of naturally occurring lyophilized N-glycans and f-mono (100 mg, 340 μmol) were dissolved in 1.0 ml of a mixed solvent (H_2O/AcOH/DMAc = 5/1/5, v/v/v). After 5 h, sodium cyanoborohydrate (62 mg, 1.0 mmol) was added to the solution. The reaction mixture was left standing at 37°C for 1.5 days and lyophilized. To the residue, 200 μl of H_2O was added. Then, the aqueous phase was washed three times with 200 μl of phenol/$CHCl_3$ (1:1, v/v). The aqueous layer was concentrated in vacuo, and excess f-mono and other chemical reagents were removed using an ODS short column attached to the kit. For comparison, the N-glycans of IgG were transformed to the 'sugar-aoWRs condensation product (*15*)' according to the manufacturer's manual. The labelled N-glycans were examined by HPLC (Pump: L-6200, HITACHI, Tokyo, Japan; Detector: FP 2020, JASCO, Tokyo, Japan; Column: COSMOSIL $5C_{18}$-PAQ Waters, Nacalai Tesque; Elution: H_2O/MeOH = 1/1, v/v), and by mass spectrometry as described above.

RESULTS AND DISCUSSION

Introducing fluorescence into the linker was accomplished by replacing the 2,6-diaminobenzene unit of our original linker molecule (mono) (*11*), with a 2,6-diaminopyridine moiety (Scheme 1). The labelling of sugar chains using 2-aminopyridine (PA) reported by Hase *et al.* (*16*) was a pioneering advance for the analysis of trace amounts of sugar-chains, and has been applied to 2- or 3-dimensional mapping by Takahashi *et al.* (*17*, *18*) for the conventional structural identification of sugar chains from natural sources, such as glycoproteins. The high fluorescence of the 2,6-diaminopyridine moiety has also been well established, and its use for the biotinylation or immobilization of sugar chains has been reported (*19*, *20*). As expected, our novel f-mono linker molecule showed fluorescence at an excitation (ex) maximum of 335 nm and an emission (em) maximum of 380 nm. Since the sensitivity of detection of fluorescence is about 1,000 times higher than that of UV/VIS, a small quantity (~1 nmol) of sugar chain can be effectively derivatized by using this f-mono linker molecule. In addition, the molecular absorption coefficient (ε value) of f-mono was five times higher than that of the original linker molecule from which it was derived, indicating increased sensitivity even with a standard UV/VIS detector.

Figure 1 shows the SPR data of Con A, RCA120 and BSA binding to α-glucose or β-galactose immobilized *via* FLCs prepared with the f-mono linker to the sensor chip. BSA was used as a negative control, because our previous investigation (*21*) showed that it does not bind to

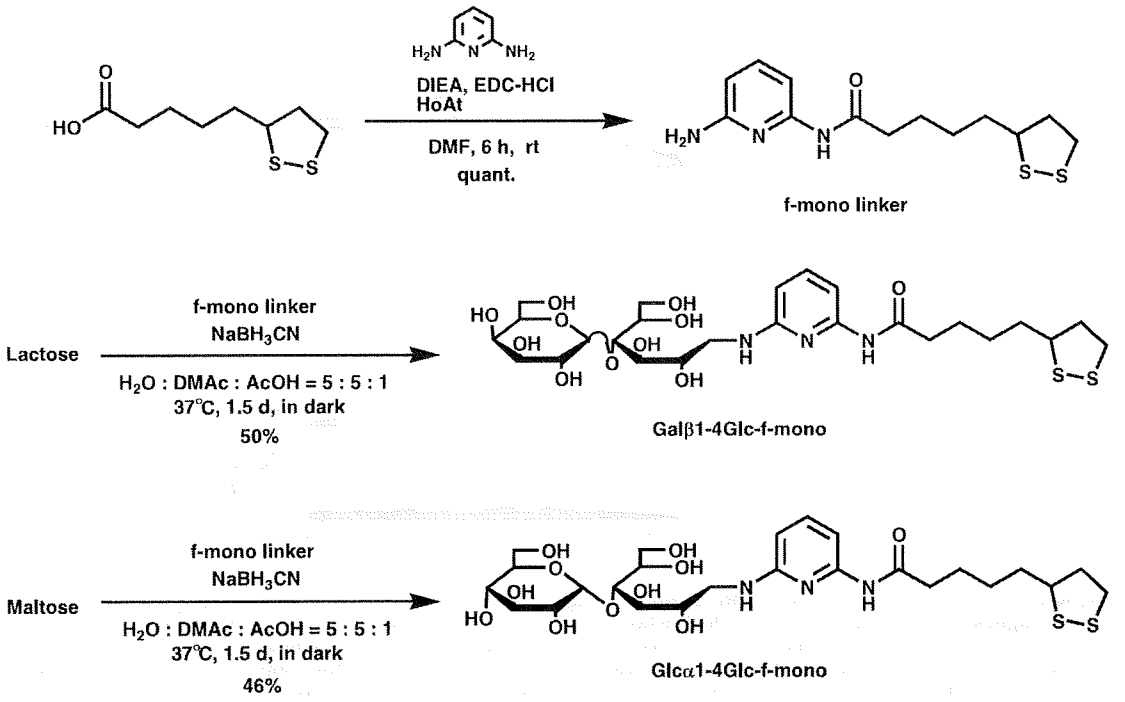

Scheme 1. **Synthesis of f-mono linker and preparation of ligand conjugates, Galβ1-4Glc-f-mono and Glcα1-4Glc-f-mono.**

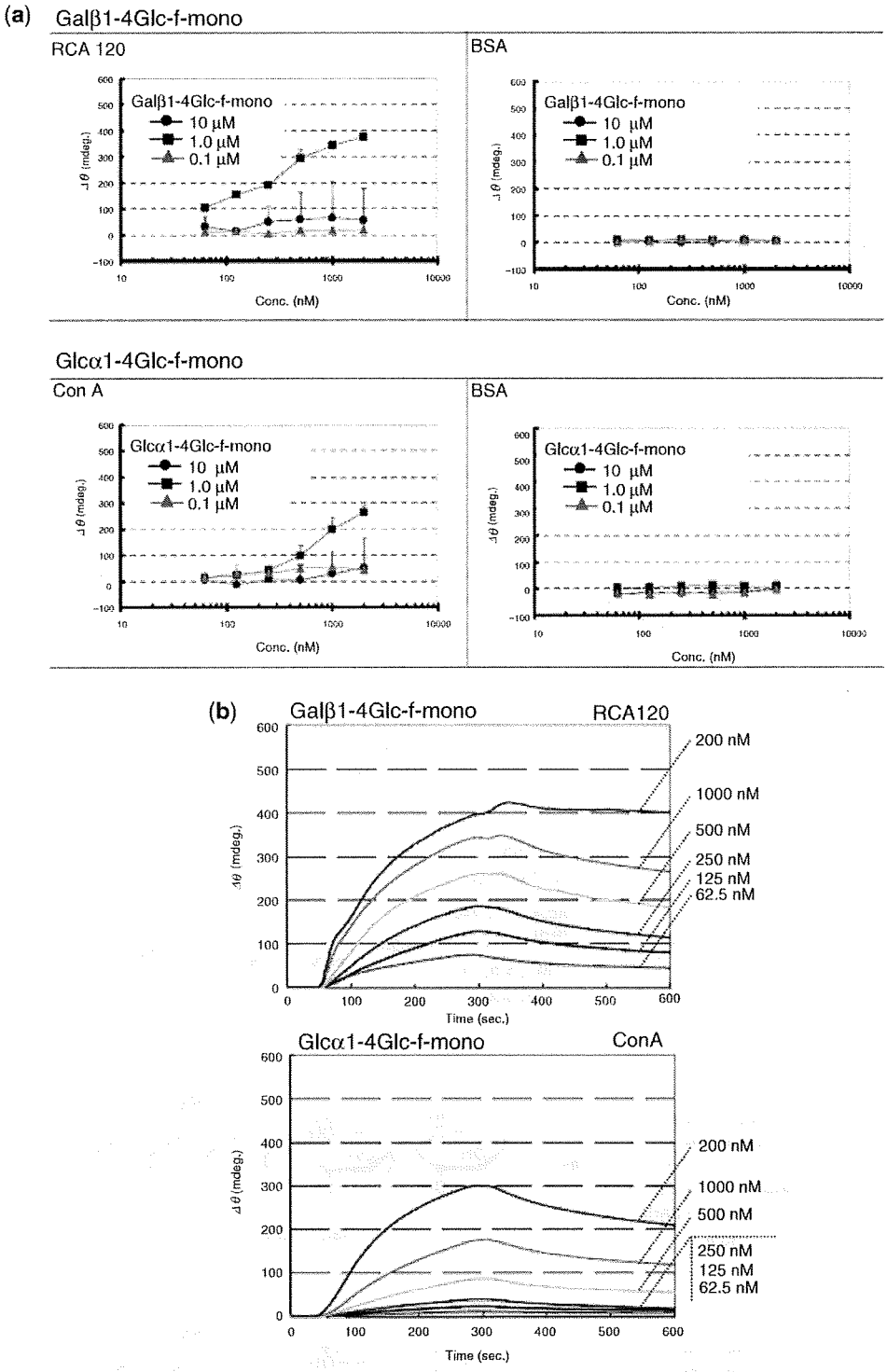

Fig. 1. **SPR analysis of lectins (Con A and RCA120) binding to defined sugars.** Galβ1-4Glc-f-mono or Glcα1-4Glc-f-mono were immobilized on gold-coated chips (see MATERIALS AND METHODS section for details). The test proteins were perfused in the aqueous phase (PBS with 0.05% Tween-20 at pH 7.4) at a flow rate of 15 μl/min at 25°C using a 12-channel SPR machine (Moritex Co., Tokyo, Japan). (a) Dependency of the lectin binding on concentration of FLCs immobilized on the chip. (b) SPR sensor grams of RCA120 for the Galβ1-4Glc-f-mono chip, and Con A for the Glcα1-4Glc-f-mono chip, immobilized at 1 μM.

α-glucose or β-galactose. Figure 1(a) illustrates the dependency of protein binding on the density of immobilization of the sugar chain *via* FLCs on the chip. The data suggest that the optimal density for immobilization of both FLCs appears to be ~1 μM. At higher concentrations, steric hindrance due to the high concentration of ligands may occur and prevent the binding of protein. At 0.1 μM of FLC the ligand sugar chains may be too diluted on the chip to effectively bind protein, because of non-clustered ligands.

Using the chip immobilized with Galβ1-4Glc-f-mono, it was detected that RCA120 bound, but Con A and BSA did not. In contrast, using the chip with Glcα1-4Glc-fmono, Con A bound, but RCA120 and BSA did not. The binding of BSA to the sensor chips was negligible.

Figure 1(b) shows typical sensorgrams of RCA120 and Con A binding to the appropriate sugar chip. The calculated binding parameters were in agreement with those in the literatures (*22*, *23*) and with our previous data using a non-fluorescent linker molecule. The kinetic parameters were; RCA120 *vs.* Galβ1-4Glc-f-mono, $k_{on} = 6.3 \times 10^3\,M^{-1}\,s^{-1}$, $k_{off} = 4.1 \times 10^{-3}\,s^{-1}$, $K_D = 0.66\,\mu M$; Con A *vs.* Glcα1-4Glc-f-mono, $k_{on} = 2.5 \times 10^3\,M^{-1}\,s^{-1}$, $k_{off} = 3.1 \times 10^{3}\,s^{-1}$, $K_D = 1.2\,\mu M$.

The results of MS and MS/MS analyses of Galβ1-4Glc-f-mono are shown in Fig. 2. A set of two unique peaks was detected. In addition to the regular $[M+H]^+$ and

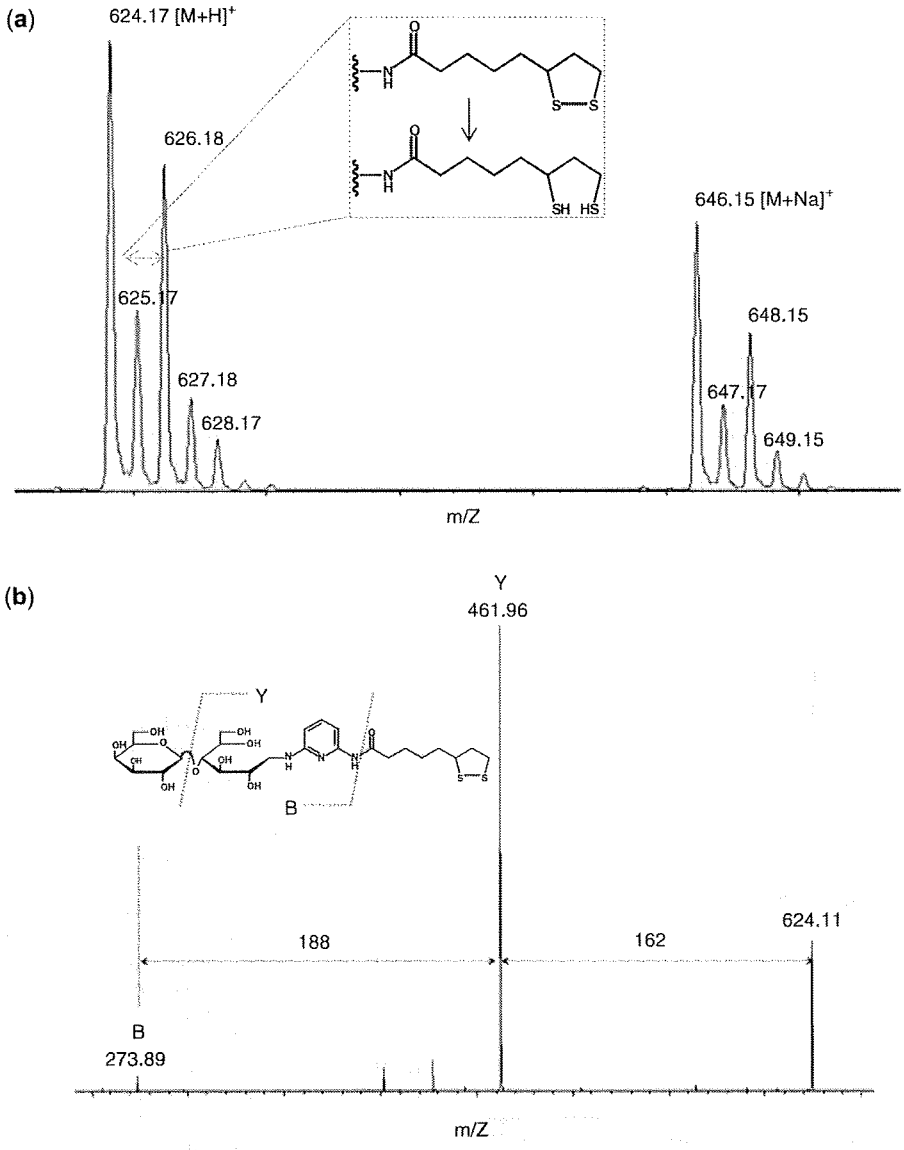

Fig. 2. **MS and MS/MS analyses of Galβ1-4Glc-f-mono.** A quadrupole ion trap and matrix-assisted laser desorption/ionization time-of-flight mass spectrometer (AXIMA-QIT) was used (see MATERIALS AND METHODS section for details). (a) MS spectrum of Galβ1-4Glc-f-mono; (b) MS/MS analysis of Galβ1-4Glc-f-mono.

$[M+Na]^+$ ion, 2-Da bigger peaks ($[M+H+2]^+$ and $[M+Na+2]^+$) were found [Fig. 2(a)]. These later peaks were derived from the reduction of the disulphide bond in the thioctic acid moiety of f-mono, since DHB (the matrix for MALDI) tends to reduce samples with the laser energy (*24*). This property of the f-mono linker was very useful for distinguishing MS peaks of f-mono-labelled glycans from contaminating peaks. In the MS/MS analysis, peaks lacking a galactose unit and thioctic acid from the precursor ion (m/z 624) were observed [Fig. 2(b)]. The cleavage here was as simple in the MS/MS analysis as that using PA-labelled sugar chains (*3*), facilitating structural analysis. For analysing structure and identifying specific sugars, the f-mono linker greatly enhanced the ability to recognize the labelled glycans. From these results, it is suggested that our f-mono linker is a highly effective reagent for MS analysis, at least in a system employing MALDI-QIT and DHBA.

Next, the N-glycans of human IgG were analysed using f-mono. As described in MATERIALS AND METHODS section, N-glycans were extracted from human IgG, concentrated, and then reacted with f-mono. Figure 3 shows the HPLC profile. Two fractions were collected and analysed using MS and MS/MS to confirm f-mono-labelled N-glycans (Fig. S1). From the MS and MS/MS, 162 or 203 different peaks were obtained, suggesting the carbohydrate-derived compounds. In addition, the f-mono labelled glycans were quite easily visualized as +2-Da differentially larger peaks in MS. From the calibration curve (Fig. S2) prepared with Galβ1-4Glc-f-mono, 518 pmol of labelled compounds were estimated to obtain from 100 μg of IgG using the HPLC results, and the detection limit in our HPLC system was estimated to be 5 pmol in 10 μl of injected sample solution.

For comparison, the released N-glycans were also labelled with a reagent (aoWRs) from the kit for MS.

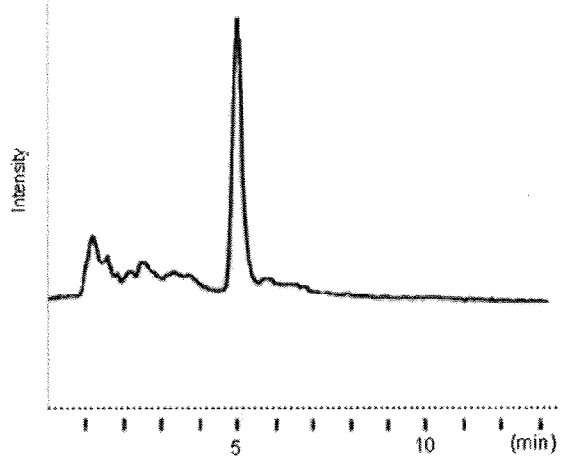

Fig. 3. **HPLC profile of f-mono labelled N-linked sugar chains from IgG.** The extraction of N-glycan and its labelling are described in the MATERIALS AND METHODS section. The conditions of HPLC were as follows. Column: COSMOSIL $5C_{18}$-PAQ Waters (Nacalai Tesque, 4.6 × 150 mm); elution: methanol/water = 1/1 (v/v).

By HPLC analysis, aoWRs-labelled N-glycans did not reveal any detectable peaks because aoWRs had no fluorescence. The MS data are summarized in Fig. 4. The MS spectrum of aoWRs-labelled N-glycans showed six glycan peaks clearly [Fig. 4(a)]. But in the case of the f-mono-labelled glycans, four additional glycans were clearly detected in the MS spectrum [Fig. 4(b)]. Furthermore, the larger 2-Da ions were observed as described above. Figure 4(c) shows the MS/MS spectrum of m/z 1947.1 ions of f-mono-labelled N-glycans. A wealth of structural information could be obtained from this spectrum. For example, from this peak the structure of the glycan containing four hexosamines and five hexoses was easily disclosed. In contrast, the MS/MS analysis of aoWRs-labelled glycan was not possible (data not shown).

The fluorescent intensity of the f-mono reagent was about 1/3 compared to that of 6-aminopyridine (PA) at the same concentration. Therefore, as judged by fluorescent intensity alone, the f-mono reagent is less sensitive. PA-derivatized sugar chains can be analysed by MS, but the f-mono derivatized one can be more easily detected because +2 Da differentially larger peaks are seen every time. Therefore, the novelty of this f-mono reagent is not the improvement of fluorescent sensitivity, but the significant improvement in MS peak identification. Moreover, the derivatized and analysed sugar chain with f-mono can be immobilized on SPR sensor chip sequentially. That is, the extensive merit of this f-mono reagent is that a more-comprehensive and integrated analysis of sugar chains can be sequentially performed using HPLC, MS and SPR.

The difficulty of synthesizing rigorously, structurally defined sugar chains remains a significant challenge to structure–function studies of carbohydrates. Narimatsu and colleagues (*25*) have made important advances in the preparation of sugar-chains using glycosyltransferases, and this synthetic approach holds promise. However, at this time, it is still challenging to prepare large, complex sugar chains. Therefore, for structure–function analyses, approaches that are economical in their use of scarce sugar chains have advantages. One solution is the SPR sugar-chip approach we have illustrated here. By immobilizing the sugar chains on the chip one can use it multiple times. In this case, it is a key to have an efficient linker molecule for immobilization of trace amounts of the defined sugar chain, of which the f-mono linker molecule is a good example.

In conclusion, the f-mono linker molecule is easily synthesized and its ligand-conjugates are easily purified. The labelled glycans are able to be traced with HPLC because of their fluorescence, making this a good application for trace amounts of glycan (~1 pmol/μl). Furthermore, the labelled glycan can be used for binding experiments using SPR, as we have previously demonstrated with non-fluorescent linker-conjugates. MS and MS/MS analyses of f-mono-labelled glycan were possible and effective in determining the glycan's primary structure, because the larger 2-Da ion peaks could be used to distinguish the labelled glycan-derived peaks. With this novel linker molecule, both the structural and functional binding analysis of trace amount of glycans are greatly facilitated, suggesting that this fluorescent linker

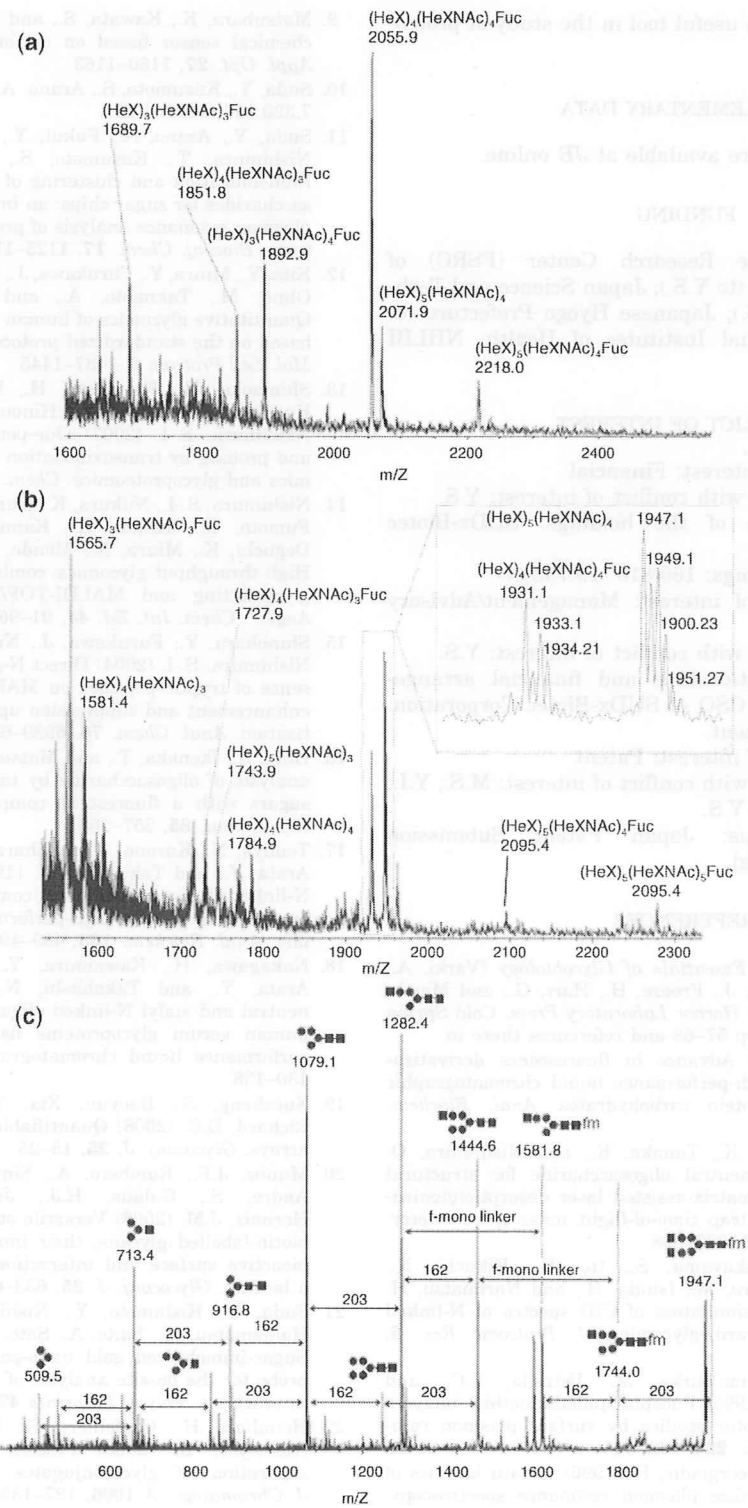

Fig. 4. **MS and MS/MS analyses of labelled N-linked sugar chains from IgG.** From 100 μg of human IgG, N-linked sugar chains were liberated by PNGase F, and concentrated by Blot Glyco (Sumitomo Bakelite Co., Ltd. Tokyo, Japan). The N-glycans were then released in H_2O, lyophilized and transformed to f-mono labelled or aoWRs conjugates as described in MATERIALS AND METHODS section. The labelled N-glycans were examined with mass spectrometry as described above. (a) aoWRs-labelled N-glycans. (b) f-mono labelled N-glycans. (c) MS/MS analysis of a peak ($m/z = 1497.1$) from the MS of f-mono labelled N-linked sugar chain from IgG.

technology should be a useful tool in the study of proteoglycomics.

SUPPLEMENTARY DATA

Supplementary data are available at *JB* online.

FUNDING

The Frontier Science Research Center (FSRC) of Kagoshima University (to Y.S.); Japan Science and Technology Agency (to Y.S.); Japanese Hyogo Prefecture (to Y.S.); and the National Institutes of Health, NHLBI (HL079182 to M.S.).

CONFLICT OF INTEREST

Nature of conflict of interest: Financial

Name of the author with conflict of interest: Y.S.

Entity and nature of the holdings: SUDx-Biotec Corporation

Amount of the holdings: 160/810 (19.753%)

Nature of conflict of interest: Management/Advisory Affiliations

Name of the author with conflict of interest: Y.S.

Nature of the relationships and financial arrangements: President and CSO of SUDx-Biotec Corporation. No financial arrangement.

Nature of conflict of interest: Patent

Name of the author with conflict of interest: M.S., Y.I., N.A., M.B., M.W. and Y.S.

Details and status: Japan Patent Submission #2008-108561 [Pending].

REFERENCES

1. Varki, A. (1999) In *Essentials of Glycobiology* (Varki, A., Cummings, R., Esko, J., Freeze, H., Hart, G., and Marth, J., eds.), *Cold Spring Horbor Laboratory Press*, Cold Spring Harbor, New York, pp 57–68 and references there in.
2. Kalyan, R.A. (2006) Advance in fluorescence derivatization methods for high-performance liquid chromatographic analysis of glycoprotein carbohydrates. *Anal. Biochem.* **350**, 1–23
3. Ojima, N., Masuda, K., Tanaka, K., and Nishimura, O. (2005) Analysis of neutral oligosaccharide for structural characterization by matrix-assisted laser desorption/ionization quadrupole ion trap time-of-flight mass spectrometry. *J. Mass Spectrom.* **40**, 380–388
4. Kameyama, A., Nakayama, S., Ito, H., Kikuchi, N., Angata, T., Nakamura, M., Ishida, H., and Narimatsu, H. (2006) Strategy for simulation of CID spectra of N-linked oligosaccharides toward glycomics. *J. Proteome Res.* **5**, 808–814
5. Plant, A.L., Brigham-Burke, M., Petrella, E.C., and O'Shannessy, D.J. (1995) Phospholipid/alkanethiol bilayers for cell-surface receptor studies by surface plasmon resonance. *Anal. Biochem.* **226**, 342–348
6. Petrlinz, K.A. and Georgiadis, R. (1996) In situ kinetics of self-assembly by surface plasmon resonance spectroscopy. *Langmuir* **12**, 4731–4740
7. Liedberg, B., Nylander, C., and Lundstrom, I. (1983) Surface plasmon resonance for gas detection and biosensing. *Sens. Actuators* **4**, 299–304
8. Flanagan, M.T. and Pantell, R.H. (1984) Surface plasmon resonance and immunosensors. *Electron. Lett.* **20**, 968–970
9. Matsubara, K., Kawata, S., and Minami, S. (1988) Optical chemical sensor based on surface plasmon measurement. *Appl. Opt.* **27**, 1160–1163
10. Suda, Y., Kusumoto, S., Arano, A., and Sobel M., US Patent 7,320,867 (2008. 1.22).
11. Suda, Y., Arano, A., Fukui, Y., Koshida, S., Wakao, M., Nishimura, T., Kusumoto, S., and Michael, S. (2006) Immobilization and clustering of structurally defined oligosaccharides for sugar chips: an improved method for surface plasmon resonance analysis of protein-carbohydrate interactions. *Bioconj. Chem.* **17**, 1125–1135
12. Kita, Y., Miura, Y., Furukawa, J., Nakano, M., Shinohara, Y., Ohno, M., Takimoto, A., and Nishimura, S.-I. (2007) Quantitative glycomics of human whole serum glycoproteins based on the standardized protocol for liberating N-glycans. *Mol. Cell Proteom* **6**, 1437–1445
13. Shimaoka, H., Kuramoto, H., Furukawa, J., Miura, Y., Kurogochi, M., Kita, Y., Hinou, H., Shinohara, Y., and Nishimura, S.-I. (2007) One-pot solid-phase glycoblotting and probing by transoximization for high-throughput glycomics and glycoproteomics. *Chem. Eur. J.* **13**, 4797–4804
14. Nishimura, S.-I., Niikura, K., Kurogochi, M., Matsushita, T., Fumoto, M., Hinou, H., Kamitani, R., Nakagawa, H., Deguchi, K., Miura, N., Monde, K., and Kondo, H. (2005) High-throughput glycomics: combined use of chemoselective glycoblotting and MALDI-TOF/TOF Mass spectrometry. *Angew. Chem. Int. Ed.* **44**, 91–96
15. Shinohara, Y., Furukawa, J., Niikura, K., Miura, N., and Nishimura, S.-I. (2004) Direct N-glycan profiling in the presence of tryptic peptides on MALDI TOF by controlled ion enhancement and suppression upon glycan-selective derivatization. *Anal. Chem.* **76**, 6989–6997
16. Hase, S., Ikenaka, T., and Matsushima, Y. (1978) Structure analysis of oligosaccharide by tagging of the reducing end sugars with a fluorescent compounds. *Biochem. Biophys. Res. Comm.* **85**, 257–263
17. Tomiya, N., Kurono, M., Ishihara, H., Tejima, S., Endo, S., Arata, Y., and Takahashi, N. (1987) Structural analysis of N-linked oligosaccharide by a combination of glycopeptidase, exoglycosidase, and high-performance liquid chromatography. *Anal. Biochem.* **163**, 489–499
18. Nakagawa, H., Kawamura, Y., Kato, K., Shimada, I., Arata, Y., and Takahashi, N. (1995) Identification of neutral and sialyl N-linked oligosaccharide structures from human serum glycoproteins using three kinds of high-performance liquid chromatography. *Anal. Biochem.* **226**, 130–138
19. Xuezheng, S., Baoyun, Xia, Yi, L., David, F.S., and Richard, D.C. (2008) Quantifiable fluorescent glycan microarrays. *Glycoconj. J.* **25**, 15–25
20. Munoz, J.F., Rumbero, A., Sinisterra, V.J., Santos, I.J., Andre, S., Gabius, H.J., Jimenez-Barbero, J., and Hernaiz, J.M. (2008) Versatile strategy for the synthesis of biotin-labelled glycans, their immobilization to establish a bioactive surface and interaction studies with a lectin on a biochip. *Glycoconj. J.* **25**, 633–646
21. Suda, Y., Kishimoto, Y., Nishimura, T., Yamashita, S., Hamamatsu, M., Saito, A., Sato, M., and Wakao, M. (2006) Sugar-immobilized gold nano-particles (SGNP): novel bioprobe for the on-site analysis of the oligosaccharide-protein interactions. *Polym. Preprints* **47**, 156–157
22. Heimholz, H., Cartellieri, S., He, L., Thiesen, P., and Niemeyer, B. (2003) Process development in affinity separation of glycoconjugates with lectins as ligands. *J. Chromatogr. A* **1006**, 127–135
23. Itakura, Y., Nakamura-Tsuruta, S., Kominami, J., Sharon, N., Kasai, K., and Hirabayashi, J. (2007) Systematic comparison of oligosaccharide specificity of Ricinus communis agglutinin I and Eryrina lectins: a search by frontal affinity chromatography. *J. Biochem.* **142**, 459–469

24. Sekiya, S., Yamaguchi, Y., Kato, K., and Tanaka, K. (2005) Mechanistic elucidation of formation of reduced 2-aminopyridine-derivatized oligosaccharide and their application in matrix assisted desorption/ionization mass spectrometry. *Rapid Commun. Mass Spectrom.* **19**, 3607–3611

25. Shirato, H., Ogawa, S., Ito, H., Sato, T., Kameyama, A., Narimatsu, H., Zheng, X., Miyamura, T., Wakita, T., Ishii, K., and Takeda, N. (2008) Noroviruses distinguish between Type 1 and Type 2 histo-blood group antigens for binding. *J. Virol.* **82**, 10756–10767

Development 136, 2511-2521 (2009) doi:10.1242/dev.037168

Two distinct types of mouse melanocyte: differential signaling requirement for the maintenance of non-cutaneous and dermal versus epidermal melanocytes

Hitomi Aoki[1], Yasuhiro Yamada[2], Akira Hara[2] and Takahiro Kunisada[1,*]

Unlike the thoroughly investigated melanocyte population in the hair follicle of the epidermis, the growth and differentiation requirements of the melanocytes in the eye, harderian gland and inner ear – the so-called non-cutaneous melanocytes – remain unclear. In this study, we investigated the in vitro and in vivo effects of the factors that regulate melanocyte development on the stem cells or the precursors of these non-cutaneous melanocytes. In general, a reduction in KIT receptor tyrosine kinase signaling leads to disordered melanocyte development. However, melanocytes in the eye, ear and harderian gland were revealed to be less sensitive to KIT signaling than cutaneous melanocytes. Instead, melanocytes in the eye and harderian gland were stimulated more effectively by endothelin 3 (ET3) or hepatocyte growth factor (HGF) signals than by KIT signaling, and the precursors of these melanocytes expressed the lowest amount of KIT. The growth and differentiation of these non-cutaneous melanocytes were specifically inhibited by antagonists for ET3 and HGF. In transgenic mice induced to express ET3 or HGF in their skin and epithelial tissues from human cytokeratin 14 promoters, the survival and differentiation of non-cutaneous and dermal melanocytes, but not epidermal melanocytes, were enhanced, apparently irrespective of KIT signaling. These results provide a molecular basis for the clear discrimination between non-cutaneous or dermal melanocytes and epidermal melanocytes, a difference that might be important in the pathogenesis of melanocyte-related diseases and melanomas.

KEY WORDS: Melanocytes, c-KIT, KITL, Endothelin, HGF, Mouse

INTRODUCTION

Melanocytes develop from the pluripotent neural crest, which also gives rise to a number of other cell types, including neurons and glial cells of the peripheral nervous system as well as bone and cartilage cells of the head skeleton. Their immature form, called the melanoblast, migrates along characteristic pathways to various destinations, such as the dermis and epidermis, the inner ear and the choroids of the eye (for reviews, see Hall, 1999; Le Douarin and Kalcheim, 1999).

The proliferation and differentiation of melanocytes in hair follicles are closely coupled with the hair regeneration cycle. The follicular melanocytes comprise a stem cell system, and melanocyte stem cells reside in the upper permanent portion of the hair follicles throughout the hair cycle (Nishimura et al., 2002). The eye, harderian gland and ear are also abundant in melanocytes; however, unlike in the hair follicles, no obvious spatially restricted niche of melanocyte stem cells has been described in these organs (Boissy, 1999).

Numerous signaling systems and transcription factors regulate all aspects of melanocyte development. These include the Wnt signaling pathway (Ikeya et al., 1997; Dorsky et al., 2000); the G-coupled endothelin B receptor (EDNRB) and its ligand, endothelin 3 (ET3; EDN3) (Baynash et al., 1994; Hosoda et al., 1994; Pavan and Tilghman, 1994); the tyrosine kinase receptor KIT and its ligand, KITL [also known as stem cell factor (SCF) or mast cell growth factor (MGF)] (Geissler et al., 1988; Cable et al., 1995; Wehrle-Haller and Weston, 1995); the hepatocyte growth factor (HGF) and its ligand, c-MET (McGill et al., 2006; Kos et al., 1999); and the transcription factors PAX3 (Watanabe et al., 1998; Potterf et al., 2000), SOX10 (Pingault et al., 1998; Southard-Smith et al., 1998; Potterf et al., 2000) and MITF, which is a basic helix-loop-helix leucine-zipper protein (Hodgkinson et al., 1993; Opdecamp et al., 1997; Nakayama et al., 1998; Lister et al., 1999). More recently, it was reported that PTEN (Inoue-Narita et al., 2008; Sarin and Artandi, 2007), Notch (Moriyama et al., 2006; Aubin-Houzelstein et al., 2008; Osawa and Fisher, 2008), FGF2 (Weiner at al., 2007; Barsh and Cotsarelis, 2007; Yonetani et al., 2008) and BCL2 (Mak et al., 2006; Nishimura et al., 2005; McGill et al., 2002) are also involved in melanocyte development. Among the genes that encode these factors, the extensively studied signaling ligand and receptor pairs, *Kitl-Kit* and *Et3-Ednrb*, provide a particularly intriguing set, as mutations in any one of them leads to a strikingly overlapping phenotype. Thus, mice with such mutations are viable but show the early loss of cells of the melanocyte lineage, which leads to white spotting phenotypes and, sometimes, to a predominately white coat color (Baynash et al., 1994; Hosoda et al., 1994; Yoshida et al., 2001; Botchkareva et al., 2001).

Using cultures of embryonic stem (ES) cells for the induction of melanocyte differentiation in vitro, we previously investigated the requirement for EDNRB signaling throughout the entire process of melanocyte development, in association with that for KIT signaling (Aoki et al., 2005). *Kit* homozygous knockout ($Kit^{W\text{-}lacZ}/Kit^{W\text{-}lacZ}$) ES cells, which were completely defective for melanocyte development, were significantly and dose dependently compensated by the addition of ET3 in vitro, and forced expression of ET3 in the skin reduced the white spot area of Kit^{W57}/Kit^{W57} mice in vivo (Aoki et al., 2005). Although KIT and EDNRB signaling are individually indispensable for the survival and maintenance of melanocyte lineage cells, at least during a certain period of development (Yoshida et al., 1996a; Shin et al., 1999), these two signals are thought to influence each other.

[1]Department of Tissue and Organ Development, Regeneration, and Advanced Medical Science, Gifu University Graduate School of Medicine, 1-1, Yanagido, Gifu 501-1194, Japan. [2]Department of Tumor Pathology, Gifu University Graduate School of Medicine, 1-1, Yanagido, Gifu 501-1194, Japan.

*Author for correspondence (e-mail: tkunisad@gifu-u.ac.jp)

Accepted 21 May 2009

It is very typical of transgenic mice in which KITL expression in the skin is induced by the cytokeratin 14 promoter that melanocyte development in specific areas of the skin is extremely progressive, and in such mice, the nose and foot-pad regions are filled with fully pigmented melanocytes as early as the newborn stage (Kunisada et al., 1998). The molecular basis for these observations is still not clear, but it appears that the environment is not uniformly favorable for melanocyte development even under the controlled expression of a single influential factor. Instead, melanocytes may react differentially to the signal in a spatially distinctive manner and region-specific melanocyte cell types might exist.

In the present study, we compared the dependencies of non-cutaneous and cutaneous (epidermal and dermal) melanocytes on KIT, EDNRB, HGF and other signals, using various genetic and cytological approaches. The results suggested that the non-cutaneous and dermal melanocytes were not as sensitive to KIT signaling as the epidermal melanocytes and instead depended more on ET3 and HGF signaling than KIT signaling. As for the cutaneous melanocytes, experimentally induced dermal melanocytes behaved more similarly to those of non-cutaneous tissues. In the light of these findings, we propose the existence of two major melanocyte populations: KIT-sensitive cutaneous melanocytes in the epidermis and weakly KIT-sensitive non-cutaneous and dermal melanocytes. Our classification, based on the growth requirements of the melanocytes, might provide new insight into the characterization of melanocytes in various animals and into the origins of human melanocyte-related diseases.

MATERIALS AND METHODS

Animals

All animal experiments were approved by the Animal Research Committee of the Graduate School of Medicine, Gifu University. ICR mice, C57BL/6 mice and *W/W*^{v} mice were obtained from Japan SLC (Shizuoka, Japan). The following transgenic mice were maintained in our animal facility: those generated with the human cytokeratin 14 promoter (hk14) driving cytokine/growth factor cDNAs [hk14-ET3 (Yamazaki et al., 2005); hk14-KITL (Kunisada et al., 1998); hk14-HGF (Kunisada et al., 2000)]; Kit Val620Ala transgenic mice (Tosaki et al., 2006); *W*^{v}*/W*^{v} and *W/W* mice derived from *W*^{v}*/+* and *W/+* mice; DCT-lacZ transgenic mice (Mackenzie et al., 1997); and C57Bl/6 background CAG-EGFP mice (RIKEN, BRC). CAG-CAT-EGFP mice (a gift from J. Miyazaki, Osaka University, Osaka, Japan) (Kawamoto et al., 2000) were bred with *Dct*$^{tm1(Cre)Bee}$ mice (a gift from F. Beermann, Swiss Institute for Experimental Cancer Research, Epalinges, Switzerland) to generate compound heterozygotes (Yonetani et al., 2008; Osawa et al., 2005). Genotyping was performed as described previously (Guyonneau et al., 2004).

Mice were housed in standard animal rooms with food and water ad libitum under controlled humidity and temperature (22±2°C) conditions. The room was illuminated by fluorescent lights that were on from 8:00 to 20:00 hours.

Cell preparation

Postnatal day (P) 0 or P3 mice were sacrificed by decapitation and ear capsules, nose, eyes, harderian glands and skin were quickly dissected on ice. The ear capsules were dissected into very small pieces. The nasal vibrissae were collected from the opposite side of the epidermis (vibrissae hair follicle) one by one, and dissected into very small fragments. The eyes were separated into cornea, lens, and neural retina; each was dissected into very small pieces (Aoki et al., 2008a). The harderian glands were also dissected into very small fragments. These small pieces of all these tissues were treated for 30 minutes at 37°C or overnight at 4°C with 0.25% trypsin/1 mM EDTA (Invitrogen, USA), 0.1% collagenase I (Sigma-Aldrich, USA) and 1× dispase (Roche, Switzerland). The skin was treated with 0.25% trypsin/1 mM EDTA for 30 minutes at 37°C or overnight at 4°C. Then, the epidermis was peeled off the underlying dermis and each layer collected separately and dissected into very small pieces. The cells of these small pieces were dissociated by gentle pipetting, and the cell suspensions strained through 400-mesh nylon (Sansho, Japan).

Cell culture

Ten thousand cells prepared from each tissue as described above were inoculated into 6-well plates previously seeded with ST2 cells or into gelatin-coated plates and cultured in Alpha Minimum Essential Medium (Invitrogen) supplemented with 10% fetal calf serum (FCS) (Equitech-Bio, USA or Nichirei Bioscience, Japan). They were maintained under 5% CO_2 at 37°C. Then, 40 pM basic fibroblast growth factor (bFGF; FGF2) (R&D Systems, USA), 10 nM dexamethasone (Dex) (Sigma) and 10 pM cholera toxin (CT) (Sigma) were added and remained present during the culture period. The medium was changed every 3 days (Aoki et al., 2008b).

The specific inhibitors and corresponding concentrations used for cell culture were: 10 μg/ml ACK2, which is a neutralizing antibody for KIT (see final section of Materials and methods); 100 ng/ml BQ788, which inhibits EDNRB (Peptides International, USA); 5 μM γ-secretase inhibitor, which is used as a Notch inhibitor; 25 μM PD98059, a MEK kinase inhibitor; 5 μM MET kinase inhibitor, used as an HGF inhibitor; 10 μM SU1498, a VEGFR inhibitor; 10 μM SU5402, an FGFR inhibitor; 10 μM AG1433, an EGFR inhibitor; and 5 μM SB203580, a p38 inhibitor (all from Merck, Germany).

Flow cytometric analysis and cell sorting

Cell suspensions of ear capsules, vibrissae, choroid, harderian glands, epidermis and dermis prepared from P0 DCT-lacZ mice or P3 *Dct*$^{tm1(Cre)Bee}$/CAG-CAT-EGFP mice as described above were centrifuged and resuspended in staining medium [SM, PBS containing 3% fetal calf serum (FCS)]. The dissociated cells were then blocked with rat anti-mouse Fc gamma receptor (2.4-G2, BD Bioscience) on ice for 30-40 minutes. After another wash with SM, the cells were stained with phycoerythrin (PE)-conjugated rat anti-mouse CD45 (PTPRC) (30-F11, BD Bioscience) on ice for 30-40 minutes, washed, and incubated with allophycocyanin (APC)-conjugated rat anti-mouse c-KIT (2B8, BD Bioscience) on ice for 30-40 minutes. The cells were washed and resuspended in SM containing 3 mg/ml propidium iodide (PI) (Calbiochem, USA). All cell sorting and analyses were performed with a FACS Aria dual-laser flow cytometer (BD Bioscience). The sorted cells were directly inoculated into 6-well plates previously seeded with ST2 stromal cells using the ACDU System (BD Bioscience).

Histology

Mice were killed with an overdose of sodium pentobarbital (200 mg/kg). The eyes were enucleated and fixed by immersion overnight in 10% formalin in phosphate buffer (pH 7.2). The methods used for histological analysis have been described in detail previously (Aoki et al., 2008c). Briefly, eyes were dehydrated with ethanol, soaked in xylene and embedded in paraffin. Horizontal serial sections were prepared at 3 μm and stained with Hematoxylin and Eosin (HE).

lacZ staining

lacZ staining was performed as reported in detail previously (Yoshida et al., 1996b). In brief, cells were fixed for 10 minutes in 2% paraformaldehyde supplemented with 0.2% glutaraldehyde and 0.02% Tween 20. After three washes in PBS, the cells were stained overnight at 37°C in 10 mM phosphate buffer (pH 7.2) containing 1.0 mM $MgCl_2$, 3.1 mM $K_4[Fe(CN)_6]$, 3.1 mM $K_3[Fe(CN)_6]$ and 2 mg/ml X-Gal. The staining reaction was stopped by washing in PBS. The specimens were post-fixed overnight in 10% formalin in phosphate buffer (pH 7.2).

Production and microinjection of monoclonal antibody

The rat monoclonal antibody ACK2 against the c-KIT receptor protein, which can block c-KIT function, and its class-matched control monoclonal antibody were described previously (Nishikawa et al., 1991).

The ACK2 antibody was microinjected into each fetal amniotic cavity at embryonic day (E) 11-12.5 as previously described (Yoshida et al., 1993). In brief, 1 μl of antibody solution (0.2-40 mg/ml) was injected into each amniotic cavity of pregnant females with a glass micropipette of ~50-70 μm diameter. The pipette was manually inserted anywhere in the

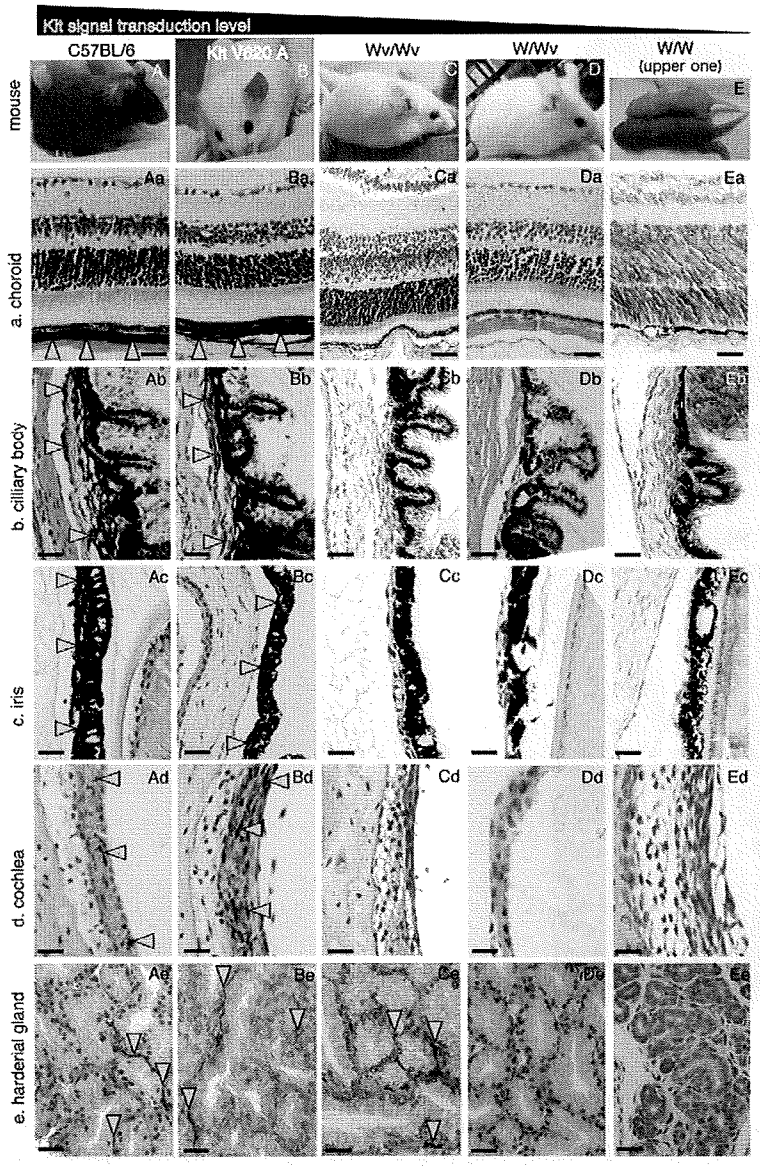

Fig. 1. Differential KIT signaling and melanocyte distribution in *Kit* mutant transgenic mice. (**A-Ee**) C57BL/6 (A), Kit V620A (B), W^v/W^v (C), W/W^v (D) and W/W (pink pup at top of E, with wild-type littermate pup beneath it) mice, arranged from left to right according to the decrease in the KIT signal level. Melanocyte localization is shown in the uvea, including the choroid (Aa-Ea), ciliary body (Ab-Eb) and iris (Ac-Ec), and in the cochlea (Ad-Ed) and harderian gland (Ae-Ee). For example, melanocytes exist not only in hair follicles, but also in the uvea including the choroid (Aa), ciliary body (Ab) and iris (Ac), as well as in the cochlea (Ad) and harderian gland (Ae), in C57Bl/6 control mice. By contrast, W/W^v (D) and W/W (E) mice had no melanocytes in their hair follicles or in any of the regions mentioned above. In W^v/W^v (C) and Kit V620A (B) mice, no melanocytes were found in the hair follicles, except in the ears. Kit V620A mice often had pigmented ears (B), and most of the non-cutaneous melanocytes in their eyes, such as those in the choroid (Ba), ciliary body (Bb), and iris (Bc), as well as melanocytes in the cochlea (Bd) and harderian gland (Be), developed normally. In W^v/W^v mice, melanocytes were detected in the harderian gland. Arrowheads indicate the melanocytes. Scale bars: 25 μm, except 50 μm in Aa-Ea.

antimesometrial third of the embryo beneath the placenta. Some of the fetuses that received a high concentration of ACK2 (e.g. over 15-20 mg/ml) died as embryos or around birth. Some surviving littermates treated with this procedure were maintained for more than 1.5 years to observe the long-term effect of the antibody treatment on coat color spotting patterns, the stability of the pattern with age and fertility, and to monitor for any behavioral abnormalities.

RESULTS

Distribution of non-cutaneous melanocytes in *Kit* coat color mutants

A mouse model of human piebaldism comprising the Val620Ala mutation in the *Kit* gene shows various coat-pigmentation patterns among the transgenic lines generated (Kit^{V620A}Tg–1 and Kit^{V620A}Tg –4) (Tosaki et al., 2006). Occasionally, phenotypes varied within the same transgenic line. For example, in Kit^{V620A}Tg –4, which is a relatively less pigmented line, we sometimes found almost completely white individuals (Fig. 1B). Spontaneous *Kit* mutants, such as *W/+* and $W^v/+$, also had white spots, and homozygous *W/W*, W^v/W^v or W/W^v mice showed a completely white coat color (Fig. 1C-E).

For these mice, which exhibit different KIT signal transduction levels, we investigated the localization of melanocytes, especially those in the non-cutaneous tissues such as the uvea (i.e. the choroid, ciliary body and iris), the cochlea and the harderian gland. C57BL/6 and Kit^{V620A}Tg, W^v/W^v, W/W^v and *W/W* mutant mice are arranged in Fig. 1 from left to right in accordance with the expected KIT signal transduction level, under which are shown histological representations of melanocytes in their choroid, ciliary body, iris, cochlea and harderian gland. Melanocytes were present in all these tissues of C57BL/6 control mice (Fig. 1Aa-e), whereas no melanocytes were found in the same tissues from W/W^v or *W/W* mice (Fig. 1Da-e,Ea-e). In Kit^{V620A}Tg mice, although they had no melanocytes in their hair follicles, melanocytes were detected in the ear capsules, and the melanocytes in their eyes (choroid, ciliary body, iris and harderian gland), as well as those in the cochlea in the

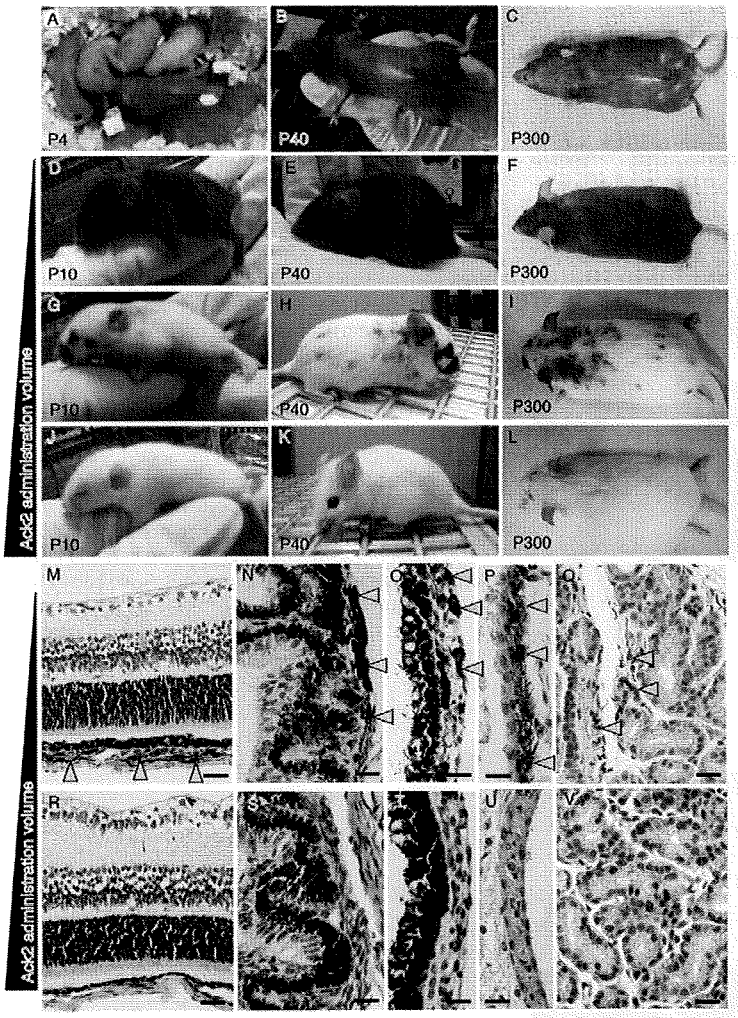

Fig. 2. KIT signal blockade with various doses of ACK2 and effects on melanocyte development. (**A-L**) Mice administered ACK2 on E12 were observed at P4, P10, P40 and P300 as labeled. (**M-V**) Hematoxylin and Eosin (HE) staining of choroid (M,R), cillia (N,S), iris (O,T), cochlea (P,U) and harderian gland (Q,V). Arrowheads indicate the melanocytes. Administration of the KIT antagonistic antibody ACK2 (20 μg) into E12 C57BL/6 mouse fetuses eliminated whole melanocyte populations including non-cutaneous melanocytes (J-L,R-V). A reduced amount of ACK2 (0.5-10 μg) allowed the differentiation of non-cutaneous melanocytes, whereas differentiation of epidermal skin melanocytes was mostly blocked (G-I,M-Q). A control mouse, which was administered with very little ACK2 (D-F), often had a small white spot only on its belly (B,C). Scale bars: 25 μm, except 50 μm in M,R.

inner ear, were found to be distributed normally (Fig. 1Ba-e). In W^v/W^v mice, which also had no melanocytes in their hair follicles, there were no melanocytes in their eyes (choroid, ciliary body and iris) or in their cochlea (Fig. 1Ca-d); however, melanocytes were distributed normally in their ear capsules and harderian gland (Fig. 1Ce). Based on these observations, we hypothesize that these non-cutaneous melanocytes might be less dependent on KIT signaling than the follicular melanocytes, although extensive loss of KIT signals does lead to a complete lack of these non-cutaneous melanocytes.

Development of non-cutaneous melanocytes after temporary inhibition of KIT signaling

To estimate the requirements for KIT signaling in the non-cutaneous mealnocytes, we utilized a neutralizing antibody for the KIT receptor, ACK2, to temporarily inhibit the KIT signaling (Nishikawa et al., 1991). C57BL/6 mice injected with ACK2 (0.2-40 μg) at E11.5-12 lost melanocyte stem cells either partially or completely, a loss that was proportional to the amount of ACK2 injected, as judged by the area of the white spots (Fig. 2; see also Materials and methods). The pigment patterns of these mice remained unchanged throughtout their life (Fig. 2A-L). Among these, completely white mice injected with more than 15 μg of ACK2 had no melanocytes in their ear capsule (Fig. 2J-L), inner ear (Fig. 2U), choroid (Fig. 2R), ciliary body (Fig. 2S), iris (Fig. 2T) or harderian gland (Fig. 2V), whereas the partially pigmented mice injected with 0.5-10 μg of ACK2 had melanocytes in theses areas (Fig. 2G-I,M-Q, arrowheads), in almost the abundance seen in the control C57BL/6 mice (Fig. 1A). These data further support the notion that non-cutaneous melanocytes are less dependent than epidermal melanocytes on KIT signaling during development.

Differential reaction of non-cutaneous melanocytes to ET3 and HGF signaling

Our previous study using transgenic mice generated with *Kitl*, *Et3* or *Hgf* cDNAs driven by the human cytokeratin 14 (*KRT14*) promoter (denoted hk14) indicated that the expression of KITL in the skin induced epidermal skin melanocytosis (Fig. 3C,G,K) and that the expression of ET3 or HGF induced dermal skin melanocytosis (Kunisada et al., 1998; Yamazaki et al., 2005; Kunisada et al., 2000) (Fig. 3A,B,E,F,I,J). Therefore, we determined the effect of the overexpression of these factors on the non-cutaneous melanocytes in the harderian glands of these transgenic mice.

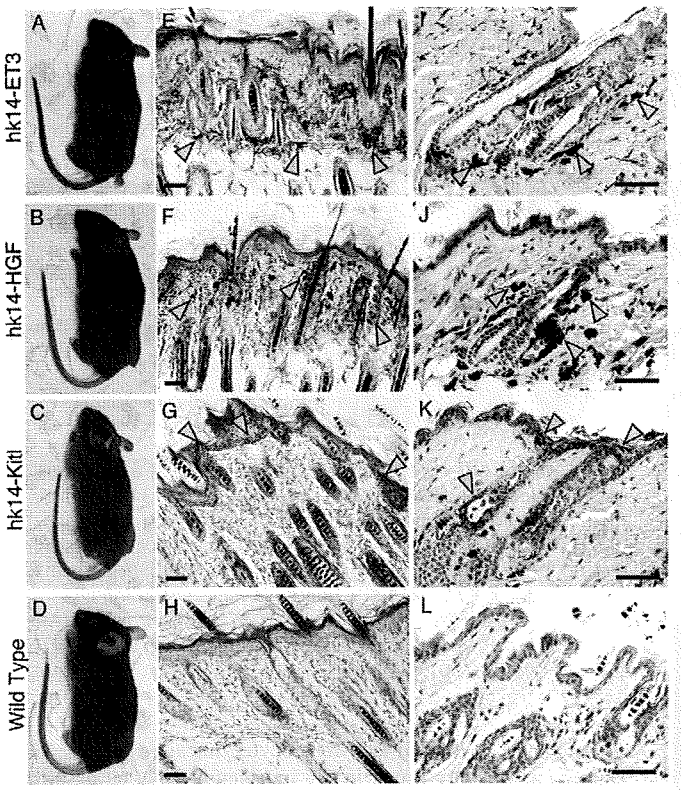

Fig. 3. Melanocyte localization in cutaneous tissue in hk14-HGF, hk14-ET3 and hk14-KITL transgenic mice. (**A-D**) hk14-ET3 (A), hk14-HGF (B) and hk14-KITL (C) transgenic mice and C57Bl/6 wild-type control (D). (**E-L**) Skin sections from hk14-ET3 (E,I), hk14-HGF (F,J) and hk14-KITL (G,K) transgenic mice, and from C57Bl/6 wild-type control (H,L). (I-L) High-magnification views (of different sections from those shown in E-H). Arrowheads indicate pigmented melanocytes sustained in the dermis (E,F,I,J) and epidermis (G,K) of adult mouse skin. Scale bars: 50 μm.

Overall, the melanocytes in the harderian glands were increased in number in these transgenic mice (Fig. 4). In hk14-ET3 mice, the number of melanocytes in the harderian gland was increased (Fig. 4A,E,I), and a significant increase was also observed in hk14-HGF mice (Fig. 4B,F,J), whereas only a slight increase was observed in hk14-KITL mice (Fig. 4C,G,K,Q). In vitro colony formation from the dissociated cells from the dissected harderian gland tissues also revealed that the number of colonies formed was dramatically increased in hk14-ET3 and hk14-HGF mice (Fig. 4M,N), with only a slight increase in hk14-KITL mice (Fig. 4O,R), as compared with the control (Fig. 4P).

In the ocular tissues, the cornea is usually clear, and we observed no melanocytes in the control C57BL6 mice (n=20/20). However, in hk14-ET3 mice we found that dendritic melanocytes had migrated into the cornea (n=20/20; Fig. 5A,D,G,J). Also, pigmented melanocytes, which were not dendritic in shape, were detected in hk14-HGF mice (n=18/20; Fig. 5B,E,H,K). In hk14-KITL mice, we never observed melanocytes in the cornea (n=20/20; Fig. 5C,F,I,L). These observations indicate that transgenically supplied KITL is less effective for the development of non-cutaneous melanocytes of the ocular tissues or harderian gland than ET3 or HGF supplied in the same manner.

Reduced expression of KIT in the non-cutaneous melanocyte precursors and their reduced response to KIT signaling compared with the cutaneous melanocyte precursors

To investigate the molecular basis of the relative ineffectiveness of KITL in the development of non-cutaneous melanocytes, we analyzed KIT expression in the cutaneous and non-cutaneous melanocytes. We previously reported that $KIT^+/CD45^-$ cells in the neonatal skin comprised the developing melanoblast population (Kunisada et al., 1996; Motohashi et al., 2007). In the cutaneous tissues, such as the epidermis, dermis, ear capsule and vibrissa, $KIT^+/CD45^-$ populations were clearly detected by flow cytometry (Fig. 6A-E). However, fewer $KIT^+/CD45^-$ cells were observed in non-cutaneous tissues, such as the uvea in the eye and harderian gland, and the average fluorescence intensity, which indicates the amount of KIT expressed on the cell surface, was clearly reduced in these tissues (Fig. 6F,G). This finding suggests that the lower expression of KIT in the melanocytes of these non-cutaneous tissues is responsible for their lower dependence on KIT signaling.

To further test the differentiation of non-cutaneous melanocytes with respect to KIT expression, we purified 1000 $KIT^+/CD45^-$ cells from P0 DCT-lacZ mice (Mackenzie et al., 1997) and cultured them on ST2 cells (Yamane et al., 1999). After 14 days, pigmented melanocytes and DCT-lacZ-positive melanoblasts were detected among the $KIT^+/CD45^-$ precursors isolated from cutaneous tissues such as the epidermis, dermis, vibrissa and ear capsule, whereas only a few pigmented melanocytes and DCT-lacZ-positive melanoblasts were generated from non-cutaneous tissues such as the uvea and harderian gland (Fig. 7A,B). Most of the colonies generated contained *lacZ*-positive cells, thus confirming the melanocyte cell lineage (Fig. 7B). Thus, very few melanocyte precursors were present in KIT^+ populations in the non-cutaneous tissues.

As we observed a number of non-pigmented but *lacZ*-positive melanoblasts in the neonatal harderian gland of DCT-lacZ mice (see Fig. S1A in the supplementary material), we dissected small pieces of harderian gland from P0 mice and cultured them without stromal cells. Successive observations every other day revealed an increase in the number of pigmented melanocytes by this culture method (see Fig. S1B in the supplementary material). Observation every 12

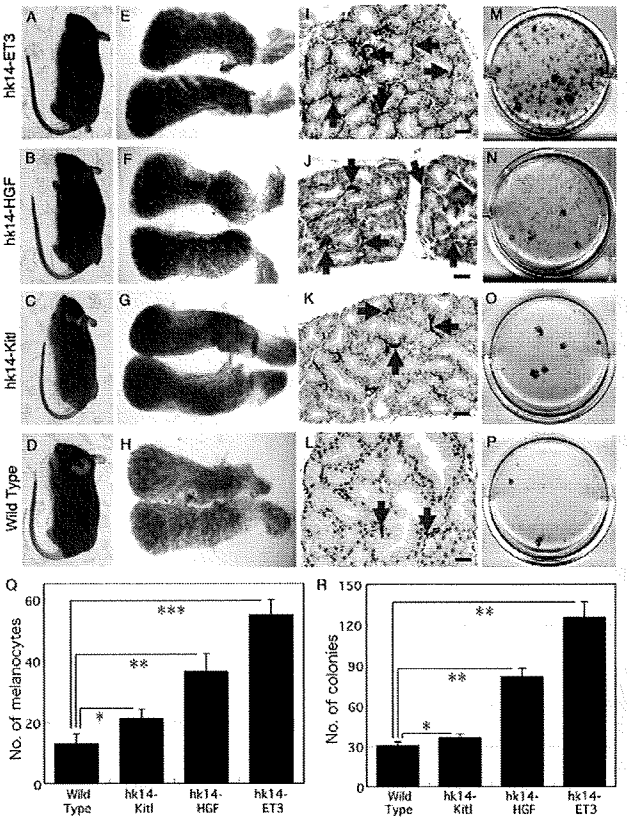

Fig. 4. Effect of exogenous ET3, HGF and KITL expression on melanocyte development in the harderian gland. (**A-P**) hk14-ET3 (A,E,I,M), hk14-HGF (B,F,J,N) and hk14-KITL (C,G,K,O) transgenic mice and C57Bl/6 as wild-type control (D,H,L,P). (A-D) Transgenic and control mice. (E-H) Oil Red O staining of harderian gland of each mouse line at P2. (I-L) HE staining of harderian gland at P19. Blue arrows indicate melanocytes. (M-P) Fourteen-day cultures of P0 harderian gland on gelatin-coated dishes. (**Q**) Number of melanocytes per microscope field of the harderian gland sections. The data are averages from three different mice. *, $P<0.05$; **, $P<0.001$; ***, $P<0.00005$. (**R**) Number of colonies constituting more than 20 melanocytes from harderian glands. The data are averages from three different mice. *, $P<0.05$; **, $P<0.0005$. Scale bars in I-L: 50 μm.

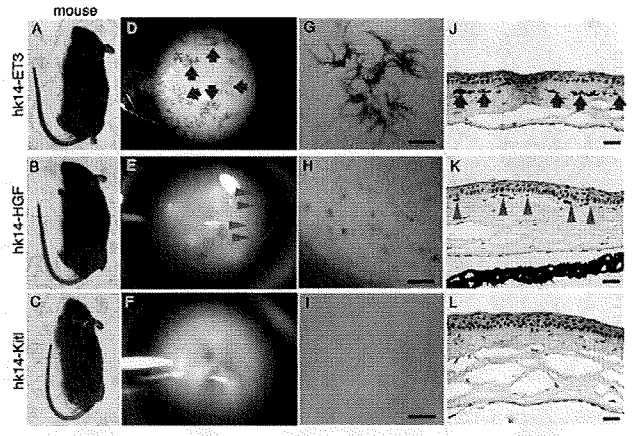

Fig. 5. Melanocytes in the cornea and the effect of exogenous expression of ET3, HGF and KITL. (**A,D,G,J**) hk14-ET3 transgenic mouse showing invasion of melanocytes into the cornea (arrows). (**B,E,H,K**) hk14-HGF transgenic mouse with the evidence of invasion of melanocyte-like, but not dendritic, pigmented cells into the cornea (arrowheads). (**C,F,I,L**) hk14-KITL transgenic mouse, showing no invasion of melanocytes into the cornea. Each transgenic mouse (A-C), its eye (D-F), cornea (G-I) and HE-stained corneal section (J-L) are shown. Scale bars: 50 μm.

hours revealed that black pigmented melanocytes present at the start of the culture did not divide actively (see Fig. S2A in the supplementary material). Pigmented cells marked in 36-hour cultures only divided once or twice in 264 hours (see Fig. S2B,C in the supplementary material). Thus, it is likely that the highly proliferative melanocyte lineage cells were not mature melanocytes and that the harderian gland or eye contained unpigmented melanoblasts. To further investigate the identity of these non-cutaneous melanoblasts, we tested whether the DCT-positive melanocyte lineage cells that were negative for the KIT receptor were really present as melanocyte precursors. For this purpose, transgenic mice were generated by crossing *Dct-Cre* knock-in mice [$Dct^{tm1(Cre)Bee}$] (Guyonneau et al., 2004) with CAG-CAT-EGFP reporter mice (Kawamoto et al., 2000) that express green fluorescent protein (GFP) under the control of a strong ubiquitous promoter (*CAG*) after Cre-mediated removal of a floxed chloramphenicol acetyl transferase (*CAT*) gene cassette so as to specifically label melanoblasts with GFP. Melanocyte lineage-specific GFP expression was confirmed in the transgenic mice, as described previously (Osawa et al., 2005). From these mice, we sorted 1000 GFP^+ cells from the $CD45^-/KIT^-$ gated population by FACS (Fig. 7C,D) and cultured them on ST2 monolayers for 14 days. From both harderian gland and ocular tissues, pigmented melanocytes were induced from the GFP^+ population; however, no melanocyte colony was detected from GFP^- cells in the $CD45^-/KIT^-$ population (Fig. 7E). Thus, precursors for the non-cutaneous melanocytes were mostly present as GFP^+ cells in the $CD45^-/KIT^-$ melanoblast population.

Factors responsible for the development of non-cutaneous melanocytes

To address the additional molecular signal(s) required for the growth and/or differentiation of melanocytes in non-cutaneous tissues, we tested the effect of signal inhibitors in vitro. First, we confirmed the effect of ET3 by using its receptor (EDNRB) antagonist, BQ788. When non-cutaneous melanocytes (i.e. those in harderian gland and eye) were cultured and treated with BQ788 or the ACK2 antibody, the growth and/or differentiation of the melanocytes was blocked effectively by BQ788 but not by ACK2 (Fig. 8A). Cutaneous melanocytes (i.e. epidermis) treated with the same concentration of these inhibitors totally disappeared (Fig. 8B). The numbers of melanocytes derived from the harderian gland and uvea were partially reduced by ACK2 treatment, but were stably maintained over a 1-50 μg/ml concentration range (Fig. 8C,D); by contrast, the number of melanocytes derived from the epidermis was sharply reduced at higher ACK2 concentrations (Fig. 8E). These results are consistent with those shown in Fig. 2, which indicated that non-cutaneous melanocytes can survive when treated with an amount of ACK2 that is effective in blocking the cutaneous melanocytes.

To investigate whether there are factors crucial for the growth and differentiation of non-cutaneous melanocytes in addition to KITL and ET3, we added various inhibitors to melanocyte cultures

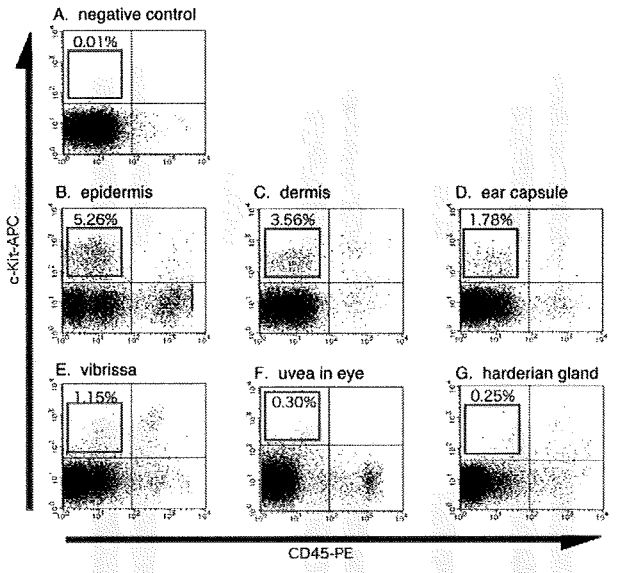

Fig. 6. Flow cytometric analysis and cell sorting of KIT⁺/CD45⁻ cells from cutaneous and non-cutaneous tissues. (**A-G**) By use of KIT-APC and CD45-PE, the percentage of KIT⁺/CD45⁻ cells (melanoblasts) was analyzed in the epidermis (B), dermis (C), ear capsule (D), vibrissa (E), uvea (F) and harderian gland (G); A shows a negative control.. The percentage of KIT⁺/CD45⁻ cells is shown in the top-left quadrant of each panel.

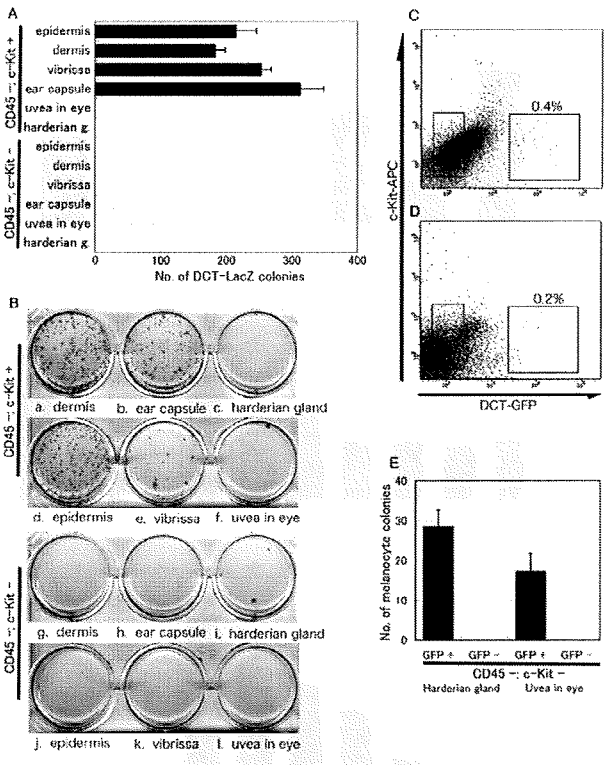

Fig. 7. In vitro differentiation of KIT⁺/CD45⁻ melanoblasts. (**A**) Number of DCT-lacZ-positive colonies generated after 14 days in cultures started from 1000 KIT⁺/CD45⁻ or KIT⁻/CD45⁻ cells sorted from the indicated tissues of P0 mice. (**B**) Dishes representative of the data shown in A. One thousand KIT⁺/CD45⁻ (**a-f**) or KIT⁻/CD45⁻ (**g-l**) cells purified by cell sorting were inoculated onto a monolayer of ST2 stromal cells. KIT⁺/CD45⁻ cells, but not KIT⁻/CD45⁻ cells, included melanoblasts in the dermis (a,g), ear capsule (b,h), epidermis (d,j) and vibrissae (e,k), but not in non-cutaneous tissue [harderian gland (c,i), uvea (f,l)]. The uvea and harderian gland contained fewer than one cell per thousand that generated DCT-lacZ-positive colonies in vitro. (**C,D**) Flow cytometric analysis of GFP⁺ cells among the KIT⁻/CD45⁻ cells in the harderian gland (C) and uvea (D). The percentage of GFP⁺ cells in the KIT⁻/CD45⁻ fractions in each panel is shown. (**E**) Number of melanocyte colonies derived from 1000 sorted cells from the GFP⁺ or GFP⁻ populations indicated in C and D.

prepared from P0 DCT-lacZ mice. When melanocytes from the harderian gland were cultured and exposed to an effective amount of PD98059, which is a MEK kinase inhibitor, or to a MET kinase inhibitor that inhibits HGF signaling, their growth and/or differentiation was severely inhibited (Fig. 9). PD98059 was effective toward all melanocyte populations tested (Fig. 9). However, the MET kinase inhibitor was more suppressive toward melanocytes from non-cutaneous tissues (Fig. 9E,F) than toward those from cutaneous tissues (Fig. 9A-D), indicating a role for HGF in the development of non-cutaneous melanocytes. Other inhibitors tested, including γ-secretase inhibitor, VEGFR (KDR) inhibitor (SU1498), FGFR inhibitor (SU5402), EGFR inhibitor (AG1433), p38 (MAPK14) inhibitor (SB203580) and Rho/Rock inhibitor (Y27632), did not show a statistically significant inhibitory effect on the melanocyte populations tested (see Fig. S3 in the supplementary material).

Further evidence for distinct epidermal and dermal melanocyte cell types

In the melanocytosis model hk14-ET3 and hk14-HGF transgenic mice, the melanocytes were maintained mostly in the dermis, whereas those in hk14-KITL transgenic mice were restricted to the epidermis, even in the aged individuals (Fig. 3E-L). Interestingly, when hk14-ET3 or hk14-HGF mice were crossed with hk14-KITL mice, the melanocytes of the double-transgenic mice were distributed to both dermis and epidermis, as a simple superimposition of both phenotypes (Fig. 10A,B). It could be that if dermal and epidermal melanocytes and their precursors maintained in the skin were mutually compatible, i.e. dermal melanocyte precursors could be recruited to become epidermal melanocytes by the exogenous ET3, an imbalance of dermal and epidermal melanocyte distribution might occur. Thus, the phenotype of the double-transgenic mice suggests the fairly discriminate and independent maintenance of these two melanocyte populations.

When a hk14-ET3 or hk14-HGF mouse was crossed with a Kit^{V620A}Tg piebaldism model mouse, the coat color pattern of the double-transgenic hk14-ET3/+;Kit^{V620A}/+ Tg or hk14-HGF/+;Kit^{V620A}/+ Tg mice was indistinguishable from that of Kit^{V620A}/+ Tg or Kit^{V620A}/Kit^{V620A} Tg mice (Fig. 11D,I). However, the skin of the double-transgenic mice was heavily pigmented, even in the area covered with white hair (Fig. 11E,J). The characteristic, heavily pigmented skin pattern of hk14-ET3 and hk14-HGF mice, and the characteristic white spot of the central head region and coat color of Kit^{V620A}Tg mice, did not change during the postnatal stage (Fig. 11A-D,F-I) (Tosaki et al., 2006). Histological analysis revealed that the dermal skin of hk14-ET3/+;Kit^{V620A}/+ Tg or hk14-HGF/+;Kit^{V620A}/+ Tg mice was pigmented (Fig. 11K,L), whereas the epidermis was not. By contrast, hk14-KITL/+;Kit^{V620A}/+ Tg

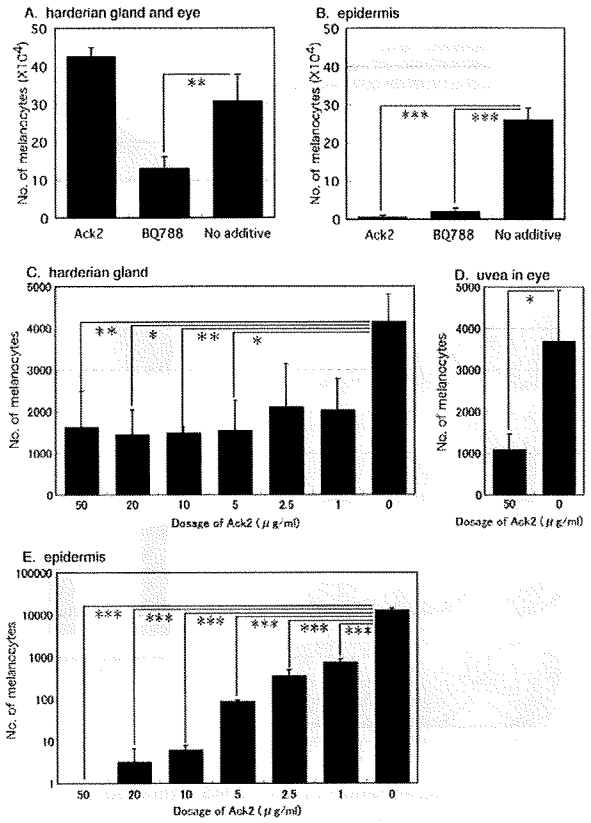

Fig. 8. Culture of P0 melanocytes with ACK2 or BQ788. (A,B) The number of melanocytes after 14 days of culturing 100,000 cells from epidermis (B) and harderian gland and uvea (A) seeded on gelatin-coated dishes and treated with effective amounts of ACK2 or BQ788. **(C-E)** ACK2 dose independency of non-cutaneous melanocytes (C, harderian gland; D, uvea) compared with the dose dependency for cutaneous melanocytes (E, epidermis). *, $P<0.05$; **, $P<0.01$; ***, $P<0.001$.

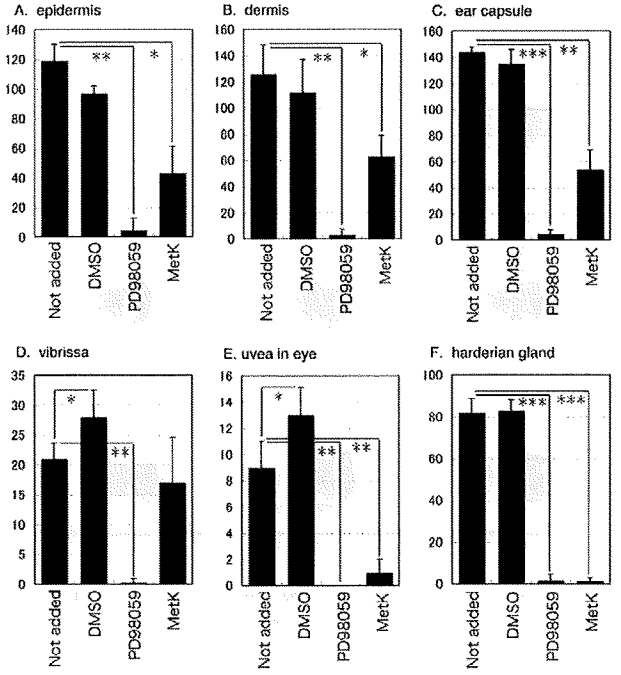

Fig. 9. Effect of inhibitors on melanocytes of various sources. Ten thousand cells from the epidermis (**A**), dermis (**B**), ear capsule (**C**), vibrissa (**D**), uvea (**E**), and harderian gland (**F**), were seeded onto monolayers of ST2 cells, and PD98059, MET kinase inhibitor (Metk), DMSO (as a vehicle control) or nothing (Not added) was added. After 14 days, the number of DCT-lacZ-positive colonies was counted. The average of three independent experiments is shown. *, $P<0.05$; **, $P<0.01$; ***, $P<0.001$.

mice with similar white spots showed pigmented skin under the black hair and totally unpigmented skin under the white hair (Fig. 11M-O). These results indicate that the ectopic localization of melanocytes in the dermis is induced and maintained by the expression of ET3 or HGF in the skin and that these dermal melanocytes do not contribute to hair pigmentation. These observations allow us to conclude that cutaneous melanocytes can be classified into two types, one being epidermal melanocytes, which are highly dependent on KIT, and the other being dermal melanocytes, which are more responsive to ET3 and HGF. As judged by their response to these factors, dermal melanocytes share the characteristics of non-cutaneous melanocytes found in the harderian glands and uvea of the eye.

DISCUSSION

Melanocytes are generally classified into cutaneous and non-cutaneous (extra-cutaneous) types. Cutaneous melanocytes are pathophysiologically distinguished as epidermal and dermal melanocytes. In this report, we described non-cutaneous melanocytes that developed in the eye, ear and harderian gland that were highly dependent on ET3 and HGF signaling and less dependent (although not totally independent) on KIT signaling, and, by contrast, epidermal melanocytes that were more dependent on KIT signaling. Cutaneous melanocytes in the dermis were revealed to be more selectively responsive to ET3 and HGF, like non-cutaneous melanocytes, and could be distinguished from epidermal melanocytes by not contributing to hair pigmentation.

In the context of the structure of skin tissue, the epidermis and dermis are composed of completely different cell populations, and therefore the cells distributed to these two regions are supposedly different in their molecular components, such as adhesion molecules, and in their growth signal dependency. Skin dendritic cells are classified into epidermal Langerhans cells and dermal dendritic cells based on differences in their cell surface marker expression patterns, gene expression profiles, growth signal requirements and immunological functions (Steinman et al., 1997). In the case of melanocytes, the expression of transgenes such as *Et3* or *Hgf* (Fig. 3) could have induced a permanent maintenance of dermal melanocytes that normally disappear after birth, indicating the specific growth requirements of dermal melanocytes. In other words, if dermal and epidermal melanocytes are of an identical cell lineage and are arbitrarily distributed among the skin tissues, then melanocyte distribution in the *Kitl* transgenic skin should have been similar to that in the *Et3* and *Hgf* transgenic mice.

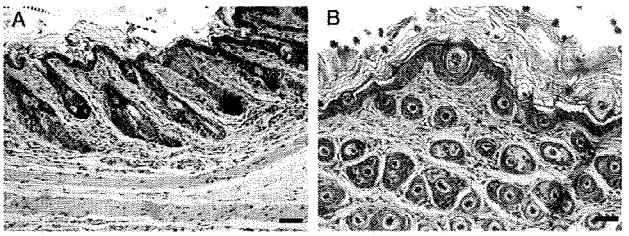

Fig. 10. Skin phenotypes of hk14-ET3/+;hk14-KITL/+ and hk14-HGF/+;hk14-KITL/+ double-transgenic mice. Skin samples from hk14-ET3/+;hk14-KITL/+ (**A**) and hk14-HGF/+;hk14-KITL/+ (**B**) double-transgenic mice were sectioned and stained with HE. Both of these double transgenic mice contain dermal and epidermal melanocytes Scale bars: 50 μm.

Dark skin (DSK) mutant mice also support our notion of distinct types of melanocyte because these mice are classified into dermal and epidermal DSK types (Fitch et al., 2003; Van Raamsdonk et al., 2004). Importantly, no DSK mutant mice are known to contain melanocytes in both their epidermis and dermis, indicating factor-specific localization of skin melanocytes. In accordance with our results, *Dsk3* and *Dsk4* (*Rps19* and *Rps20*) mutants would contain epidermal melanocytes generated by the augmented expression of skin KITL (McGowan et al., 2008). Recent identification of the uveal melanoma and blue naevi-specific mutation of the human counterpart of DSK1 (GNAQ), the heterotrimeric G-protein α-subunit, as opposed to the BRAF and NRAS mutations exclusively found in neoplasms originating from epidermal melanocytes (Van Raamsdonk et al., 2009), also indicate the distinct nature of non-cutaneous and epidermal melanocytes. Still, as suggested by Van Raamsdonk et al. (Van Raamsdonk et al., 2004), increased ET3 or HGF signaling might cause excessive proliferation of the early melanoblasts, followed by their restricted entry into the epidermis across the basal layer. In this scenario, melanocytes left behind in the dermis may develop into the dermal cell type in response to dermal-specific environmental cues.

The precise origins of the non-cutaneous and dermal melanocytes, as well as of epidermal melanocytes, are still open to further investigation. Epidermal melanocytes, including those of hair follicles, are maintained in a KITL-rich environment, whereas dermal melanocytes are supposed to be selectively maintained by

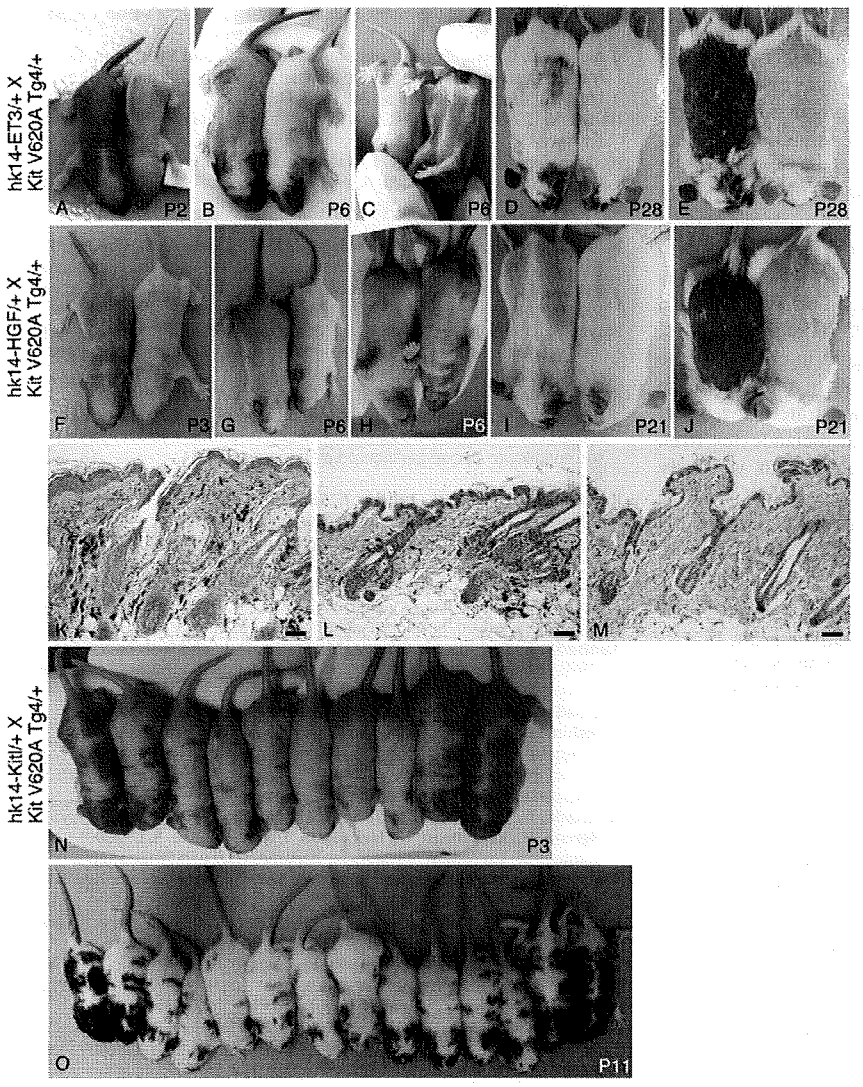

Fig. 11. Mice with pigmented dermis and white hair. (**A-E**) Mice with black pigmented dermis and white hair derived from a cross between hk14-ET3/+ and Kit V620A Tg4/+ mice (left pup in A,B,D,E and right pup in C). Photographs were taken at P2, P6 and P28 as labeled. Kit V620A Tg4/+ mice are shown alongside the double-transgenic mice. (**F-J**) Mice with black pigmented dermis and white hair derived from a cross between hk14-HGF/+ and Kit V620A Tg4/+ mice (left pup in F,G,I,J and right pup in H). Photographs were taken at P3, P6 and P21 as labeled. Kit V620A Tg4/+ mice are shown alongside the double-transgenic mice. (**K-M**) HE-stained skin samples from hk14-ET3/+;Kit V620A Tg4/+ (K) and hk14-HGF/+;Kit Tg4/+ (L) mice clearly show the absence of pigment granules in hair follicles but the presence of melanocytes in dermis, whereas hk14-KITL/+;Kit V620A Tg4/+ (M) samples show the absence of both pigment granules in hair follicles and melanocytes in dermis under the white hair. (**N,O**) Mice with black pigmented epidermis and black hair derived from a cross between hk14-KITL/+ and Kit V620A Tg4/+ mice. Photographs were taken at P3 and P11 as labeled. Scale bars: 50 μm.

ET3 or HGF expression. Since the number of epidermal melanocytes and their distribution pattern were not affected by ET3 or HGF expression (Kunisada et al., 1998; Kunisada et al., 2000) (H.A. and T.K., unpublished), common precursors for these two melanocyte populations would probably have separated from each other at a considerably early developmental stage. If not, common precursors would have been exhaustively used for the dermal melanocyte population. In addition, hk14-ET3/+;Kit^{V620A}/+ Tg mice are white in coat color and have dark pigmented dermal skin underneath, suggesting that dermal- and epidermal-restricted niches are required for each melanocyte population. This lifetime-stable localization further supports the distinct nature of these two populations. Recently, Notch signaling was reported to be selectively employed for the maintenance of epidermal melanocytes: in *Notch1* and/or *Notch2* conditional knockout mice, the ear and choroid layer were pigmented normally, in contrast to the gradual loss of coat color pigmentation (Schouwey et al., 2007). This finding also highlights the discrimination of epidermal melanocytes from dermal or non-cutaneous melanocytes.

In relation to skin diseases caused by aberrant melanocyte development, the characteristics of the melanocytes should be considered. In the case of dermal melanocytosis, a broad group of congenital and acquired melanocytic lesions (Zembowicz and Mihm, 2004), ET or HGF are more likely to be involved in the pathogenesis of this disease than is KIT signaling. However, it should also be emphasized that both melanocyte cell types are derived from common neural crest-derived precursors, as *W/W* mutation or extensive blockade of KIT signaling during embryogenesis completely eliminates the melanocytes from the whole body. In fact, we occasionally found W^v/W^v mice with white ear capsules accompanied by totally unpigmented harderian glands, in contrast to the majority of the W^v/W^v individuals with pigmentation in both their ear capsules and harderian glands (as shown in Fig. 1C). This finding might indicate a decisive effect of a small fluctuation in the KIT signal among W^v/W^v individuals, i.e. reflecting an exacting threshold of KIT signal intensity for the survival of developing melanocytes, at least in their common precursors. At the same time, we demonstrated the strict discrimination of non-cutaneous and dermal melanocytes from epidermal melanocytes based on their reactions to variously manipulated external ligands, including KITL, ET3 and HGF. These findings might help towards a clearer understanding of the pathogenesis of melanocyte-related diseases, including melanomas.

Acknowledgements

We thank Dr Shin-ichi Nishikawa for providing the ACK2 hybridoma cell line and ST2 stromal cell line, Kyoko Takahashi for her excellent technical assistance, and Drs Hisahiro Yoshida, Tsutomu Motohashi and Kenichi Tezuka for their thoughtful advice. This work was supported by JSPS Research Fellowships for Young Scientists to H.A.

Supplementary material

Supplementary material for this article is available at http://dev.biologists.org/cgi/content/full/136/15/2511/DC1

References

Aoki, H., Motohashi, T., Yoshimura, N., Yamazaki, H., Yamane, T., Panthier, J. J. and Kunisada, T. (2005). Cooperative and indispensable roles of endothelin 3 and KIT signalings in melanocyte development. *Dev. Dyn.* **233**, 407-417.

Aoki, H., Yoshida, H., Hara, A., Suzuki, T. and Kunisada, T. (2008a). Transplantation of melanocytes into iris: method for iris repigmentation. *Transplantation* **85**, 492-494.

Aoki, H., Hara, A., Motohashi, T., Chem, H. and Kunisada, T. (2008b). Iris as a recipient tissue for pigment cells: organized in vivo differentiation of melanocytes and pigmented epithelium derived from embryonic stem cells in vitro. *Dev. Dyn.* **237**, 2394-2404.

Aoki, H., Hara, A., Niwa, M., Motohashi, T., Suzuki, T. and Kunisada, T. (2008c). Transplantation of cells from eye-like structures differentiated from embryonic stem cells in vitro and in vivo regeneration of retinal ganglion-like cells. *Graefes. Arch. Clin. Exp. Ophthalmol.* **246**, 255-265.

Aubin-Houzelstein, G., Djian-Zaouche, J., Bernex, F., Gadin, S., Delmas, V., Larue, L. and Panthier, J. J. (2008). Melanoblasts' proper location and timed differentiation depend on Notch/RBP-J signaling in postnatal hair follicles. *J. Invest. Dermatol.* **128**, 2686-2695.

Barsh, G. and Cotsarelis, G. (2007). How hair gets its pigment. *Cell* **130**, 779-781.

Baynash, A. G., Hosoda, K., Giaid, A., Richardson, J. A., Emoto, N., Hammer, R. E. and Yanagisawa, M. (1994). Interaction of endothelin-3 with endothelin-B receptor is essential for development of epidermal melanocytes and enteric neurons. *Cell* **79**, 1277-1285.

Boissy, R. E. (1999). Extracutaneous melanocytes. In *The Pigmentary System* (ed. J. J. Nordlund., R. E. Boissy., V. J. Hearing., R. A. King and J. P. Ortone), pp. 59-72. New York: Oxford University Press.

Botchkareva, N. V., Khlgatian, M., Longley, B. J., Botchkarev, V. A. and Gilchrest, B. A. (2001). SCF/c-kit signaling is required for cyclic regeneration of the hair pigmentation unit. *FASEB J.* **15**, 645-658.

Cable, J., Jackson, I. J. and Steel, K. P. (1995). Mutations at the W locus affect survival of neural crest-derived melanocytes in the mouse. *Mech. Dev.* **50**, 139-150.

Dorsky, R. I., Raible, D. W. and Moon, R. T. (2000). Direct regulation of nacre, a zebrafish MITF homolog required for pigment cell formation, by the Wnt pathway. *Genes Dev.* **14**, 158-162.

Fitch, K. R., McGowan, K. A., van Raamsdonk, C. D., Fuchs, H., Lee, D., Puech, A., Hérault, Y., Threadgill, D. W., Hrabé de Angelis, M. and Barsh, G. S. (2003). Genetics of dark skin in mice. *Genes Dev.* **17**, 214-228.

Geissler, E. N., Ryan, M. A. and Housman, D. E. (1988). The dominant-white spotting (W) locus of the mouse encodes the c-kit proto-oncogene. *Cell* **55**, 185-192.

Guyonneau, L., Murisier, F., Rossier, A., Moulin, A. and Beermann, F. (2004). Melanocytes and pigmentation are affected in dopachrome tautomerase knockout mice. *Mol. Cell. Biol.* **24**, 3396-3403.

Hall, B. K. (1999). *The Neural Crest in Development and Evolution*. New York: Springer.

Hodgkinson, C. A., Moore, K. J., Nakayama, A., Steingrímsson, E., Copeland, N. G., Jenkins, N. A. and Arnheiter, H. (1993). Mutations at the mouse microphthalmia locus are associated with defects in a gene encoding a novel basic-helix-loop-helix-zipper protein. *Cell* **74**, 395-404.

Hosoda, K., Hammer, R. E., Richardson, J. A., Baynash, A. G., Cheung, J. C., Giaid, A. and Yanagisawa, M. (1994). Targeted and natural (piebald-lethal) mutations of endothelin-B receptor gene produce megacolon associated with spotted coat color in mice. *Cell* **79**, 1267-1276.

Ikeya, M., Lee, S. M., Johnson, J. E., McMahon, A. P. and Takada, S. (1997). Wnt signalling required for expansion of neural crest and CNS progenitors. *Nature* **389**, 966-970.

Inoue-Narita, T., Hamada, K., Sasaki, T., Hatakeyama, S., Fujita, S., Kawahara, K., Sasaki, M., Kishimoto, H., Eguchi, S., Kojima, I. et al. (2008). Pten deficiency in melanocytes results in resistance to hair graying and susceptibility to carcinogen-induced melanomagenesis. *Cancer Res.* **68**, 5760-5768.

Kawamoto, S., Niwa, H., Tashiro, F., Sano, S., Kondoh, G., Takeda, J., Tabayashi, K. and Miyazaki, J. (2000). A novel reporter mouse strain that expresses enhanced green fluorescent protein upon Cre-mediated recombination. *FEBS Lett.* **470**, 263-268.

Kos, L., Aronzon, A., Takayama, H., Maina, F., Ponzetto, C., Merlino, G. and Pavan, W. (1999). Hepatocyte growth factor/scatter factor-MET signaling in neural crest-derived melanocyte development. *Pigment Cell Res.* **12**, 13-21.

Kunisada, T., Yoshida, H., Ogawa, M., Shultz, D. L. and Nishikawa, S. I. (1996). Characterization and isolation of melanocyte progenitors from mouse embryos. *Dev. Growth Differ.* **38**, 87-97.

Kunisada, T., Yoshida, H., Yamazaki, H., Miyamoto, A., Hemmi, H., Nishimura, E., Shultz, L. D., Nishikawa, S. and Hayashi, S. (1998). Transgene expression of steel factor in the basal layer of epidermis promotes survival, proliferation, differentiation and migration of melanocyte precursors. *Development* **125**, 2915-2923.

Kunisada, T., Yamazaki, H., Hirobe, T., Kamei, S., Omoteno, M., Tagaya, H., Hemmi, H., Koshimizu, U., Nakamura, T. and Hayashi, S. I. (2000). Keratinocyte expression of transgenic hepatocyte growth factor affects melanocyte development, leading to dermal melanocytosis. *Mech. Dev.* **94**, 67-78.

Le Douarin, N. M. and Kalcheim, C. (1999). *The Neural Crest*, 2nd edn. New York: Cambridge University Press.

Lister, J. A., Robertson, C. P., Lepage, T., Johnson, S. L. and Raible, D. W. (1999). nacre encodes a zebrafish microphthalmia-related protein that regulates neural-crest-derived pigment cell fate. *Development* **126**, 3757-3767.

Mackenzie, M. A., Jordan, S. A., Budd, P. S. and Jackson, I. J. (1997). Activation of the receptor tyrosine kinase Kit is required for the proliferation of melanoblasts in the mouse embryo. *Dev. Biol.* **192**, 99-107.

Mak, S. S., Moriyama, M., Nishioka, E., Osawa, M. and Nishikawa, S. (2006). Indispensable role of Bcl2 in the development of the melanocyte stem cell. *Dev. Biol.* **291**, 144-153.
McGill, G. G., Horstmann, M., Widlund, H. R., Du, J., Motyckova, G., Nishimura, E. K., Lin, Y. L., Ramaswamy, S., Avery, W., Ding, H. F. et al. (2002). Bcl2 regulation by the melanocyte master regulator Mitf modulates lineage survival and melanoma cell viability. *Cell* **109**, 707-718.
McGill, G. G., Haq, R., Nishimura, E. K. and Fisher, D. E. (2006). c-Met expression is regulated by Mitf in the melanocyte lineage. *J. Biol. Chem.* **281**, 10365-10373.
McGowan, K. A., Li, J. Z., Park, C. Y., Beaudry, V., Tabor, H. K., Sabnis, A. J., Zhang, W., Fuchs, H., de Angelis, M. H., Myers, R. M. et al. (2008). Ribosomal mutations cause p53-mediated dark skin and pleiotropic effects. *Nat. Genet.* **40**, 963-970.
Moriyama, M., Osawa, M., Mak, S. S., Ohtsuka, T., Yamamoto, N., Han, H., Delmas, V., Kageyama, R., Beermann, F., Larue, L. et al. (2006). Notch signaling via Hes1 transcription factor maintains survival of melanoblasts and melanocyte stem cells. *J. Cell Biol.* **173**, 333-339.
Motohashi, T., Aoki, H., Chiba, K., Yoshimura, N. and Kunisada, T. (2007). Multipotent cell fate of neural crest-like cells derived from embryonic stem cells. *Stem Cells* **25**, 402-410.
Nakayama, A., Nguyen, M. T., Chen, C. C., Opdecamp, K., Hodgkinson, C. A. and Arnheiter, H. (1998). Mutations in microphthalmia, the mouse homolog of the human deafness gene MITF, affect neuroepithelial and neural crest-derived melanocytes differently. *Mech. Dev.* **70**, 155-166.
Nishikawa, S., Kusakabe, M., Yoshinaga, K., Ogawa, M., Hayashi, S., Kunisada, T., Era, T., Sakakura, T. and Nishikawa, S. (1991). In utero manipulation of coat color formation by a monoclonal anti-c-kit antibody: two distinct waves of c-kit-dependency during melanocyte development. *EMBO J.* **10**, 2111-2118.
Nishimura, E. K., Jordan, S. A., Oshima, H., Yoshida, H., Osawa, M., Moriyama, M., Jackson, I. J., Barrandon, Y., Miyachi, Y. and Nishikawa, S. (2002). Dominant role of the niche in melanocyte stem-cell fate determination. *Nature* **416**, 854-860.
Nishimura, E. K., Granter, S. R. and Fisher, D. E. (2005). Mechanisms of hair graying: incomplete melanocyte stem cell maintenance in the niche. *Science* **307**, 720-724.
Opdecamp, K., Nakayama, A., Nguyen, M. T., Hodgkinson, C. A., Pavan, W. J. and Arnheiter, H. (1997). Melanocyte development in vivo and in neural crest cell cultures: crucial dependence on the Mitf basic-helix-loop-helix-zipper transcription factor. *Development* **124**, 2377-2386.
Osawa, M. and Fisher, D. E. (2008). Notch and melanocytes: diverse outcomes from a single signal. *J. Invest. Dermatol.* **128**, 2571-2574.
Osawa, M., Egawa, G., Mak, S. S., Moriyama, M., Freter, R., Yonetani, S., Beermann, F. and Nishikawa, S. (2005). Molecular characterization of melanocyte stem cells in their niche. *Development* **132**, 5589-5599.
Pavan, W. J. and Tilghman, S. M. (1994). Piebald lethal (sl) acts early to disrupt the development of neural crest-derived melanocytes. *Proc. Natl. Acad. Sci. USA* **91**, 7159-7163.
Pingault, V., Bondurand, N., Kuhlbrodt, K., Goerich, D. E., Préhu, M. O., Puliti, A., Herbarth, B., Hermans-Borgmeyer, I., Legius, E., Matthijs, G. et al. (1998). SOX10 mutations in patients with Waardenburg-Hirschsprung disease. *Nat. Genet.* **18**, 171-173.
Potterf, S. B., Furumura, M., Dunn, K. J., Arnheiter, H. and Pavan, W. J. (2000). Transcription factor hierarchy in Waardenburg syndrome: regulation of MITF expression by SOX10 and PAX3. *Hum. Genet.* **107**, 1-6.
Sarin, K. Y. and Artandi, S. E. (2007). Aging, graying and loss of melanocyte stem cells. *Stem Cell Rev.* **3**, 212-217.
Schouwey, K., Delmas, V., Larue, L., Zimber-Strobl, U., Strobl, L. J., Radtke, F. and Beermann, F. (2007). Notch1 and Notch2 receptors influence progressive hair graying in a dose-dependent manner. *Dev. Dyn.* **236**, 282-289.
Shin, M. K., Levorse, J. M., Ingram, R. S. and Tilghman, S. M. (1999). The temporal requirement for endothelin receptor-B signalling during neural crest development. *Nature* **402**, 496-501.
Southard-Smith, E. M., Kos, L. and Pavan, W. J. (1998). Sox10 mutation disrupts neural crest development in Dom Hirschsprung mouse model. *Nat. Genet.* **18**, 60-64.
Steinman, R. M., Pack, M. and Inaba, K. (1997). Dendritic cell development and maturation. *Adv. Exp. Med. Biol.* **417**, 1-6.
Tosaki, H., Kunisada, T., Motohashi, T., Aoki, H., Yoshida, H. and Kitajima, Y. (2006). Mice transgenic for Kit(V620A): recapitulation of piebaldism but not progressive depigmentation seen in humans with this mutation. *J. Invest. Dermatol.* **126**, 1111-1118.
Van Raamsdonk, C. D., Fitch, K. R., Fuchs, H., de Angelis, M. H. and Barsh, G. S. (2004). Effects of G-protein mutations on skin color. *Nat. Genet.* **36**, 961-968.
Van Raamsdonk, C. D., Bezrookove, V., Green, G., Bauer, J., Gaugler, L., O'Brien, J. M., Simpson, E. M., Barsh, G. S., Bastian, B. C. (2009). Frequent somatic mutations of GNAQ in uveal melanoma and blue naevi. *Nature* **457**, 599-602.
Watanabe, A., Takeda, K., Ploplis, B. and Tachibana, M. (1998). Epistatic relationship between Waardenburg syndrome genes MITF and PAX3. *Nat. Genet.* **18**, 283-286.
Wehrle-Haller, B. and Weston, J. A. (1995). Soluble and cell-bound forms of steel factor activity play distinct roles in melanocyte precursor dispersal and survival on the lateral neural crest migration pathway. *Development* **121**, 731-742.
Weiner, L., Han, R., Scicchitano, B. M., Li, J., Hasegawa, K., Grossi, M., Lee, D. and Brissette, J. L. (2007). Dedicated epithelial recipient cells determine pigmentation patterns. *Cell* **130**, 932-942.
Yamane, T., Hayashi, S., Mizoguchi, M., Yamazaki, H. and Kunisada, T. (1999). Derivation of melanocytes from embryonic stem cells in culture. *Dev. Dyn.* **216**, 450-458.
Yamazaki, H., Sakata, E., Yamane, T., Yanagisawa, A., Abe, K., Yamamura, K., Hayashi, S. and Kunisada, T. (2005). Presence and distribution of neural crest-derived cells in the murine developing thymus and their potential for differentiation. *Int. Immunol.* **17**, 549-558.
Yonetani, S., Moriyama, M., Nishigori, C., Osawa, M. and Nishikawa, S. (2008). In vitro expansion of immature melanoblasts and their ability to repopulate melanocyte stem cells in the hair follicle. *J. Invest. Dermatol.* **128**, 408-420.
Yoshida, H., Nishikawa, S.-I., Okamura, H., Sakakura, T. and Kusakabe, M. (1993). The role of c-kit proto-oncogene during melanocyte development in mouse. In vivo approach by the in utero microinjection of anti-c-kit antibody. *Dev. Growth Differ.* **35**, 209-220.
Yoshida, H., Kunisada, T., Kusakabe, M., Nishikawa, S. and Nishikawa, S. I. (1996a). Distinct stages of melanocyte differentiation revealed by analysis of nonuniform pigmentation patterns. *Development* **122**, 1207-1214.
Yoshida, H., Hayashi, S., Shultz, L. D., Yamamura, K., Nishikawa, S., Nishikawa, S. and Kunisada, T. (1996b). Neural and skin cell-specific expression pattern conferred by steel factor regulatory sequence in transgenic mice. *Dev. Dyn.* **207**, 222-232.
Yoshida, H., Kunisada, T., Grimm, T., Nishimura, E. K., Nishioka, E. and Nishikawa, S. I. (2001). Melanocyte migration and survival controlled by SCF/c-kit expression. *J. Investig. Dermatol. Symp. Proc.* **6**, 1-5.
Zembowicz, A. and Mihm, M. C. (2004). Dermal dendritic melanocytic proliferations: an update. *Histopathology* **45**, 433-451.